

Modelling non-linear evolution using Lagrangian Perturbation Theory (LPT) re-expansions

Sharvari Nadkarni-Ghosh^{1,2*} and David F. Chernoff^{3†}

¹*Department of Theoretical Sciences, S.N. Bose N.C.B.S, Sector III, Block JD, Salt Lake, Kolkata, W.B. 700098 India*

²*Department of Physics, I.I.T. Kanpur, Kanpur, U.P. 208016 India*

³*Department of Astronomy, Cornell University, Ithaca, NY 14853 USA*

ABSTRACT

We present a new method to calculate formation of cosmological structure in the Newtonian limit. The method is based on Lagrangian perturbation theory plus two key theoretical extensions. One advance involves identifying and fixing a previously ignored gauge-like degree of freedom relating quantities calculated in LPT to those measured by a preferred Friedmann-Robertson-Walker (FRW) observer. Handling this connection between calculational and observer frames is physically essential and ensures a momentum conserving description. The second extension is to systematically re-expand the equations of motion to increase LPT’s radius of convergence to the maximum future time prior to orbit crossing. The paper implements a complete algorithm and performs extensive “proof of principle” tests of the new method, including direct comparison to known solutions, evaluation of conserved quantities and formal convergence studies. All are satisfactory. We show convergence is exponential in grid size and Lagrangian order and polynomial in step size. There are three *powerful advantages* afforded by the new technique: (1) it employs a smooth representation of all fields and the results are not limited by particle induced shot-noise errors, (2) it permits the numerical error to be controlled by changing Lagrangian order and/or number of steps allowing, in principle, arbitrarily small errors to be achieved prior to orbit crossing and (3) it handles generic cold initial data (any periodic density and velocity fields, including those with initial rotational components). Together, these properties make the new technique well-suited to handle quasi-linear scales where analytic methods and/or numerical simulations fail to provide suitably accurate answers.

Key words: cosmology: theory – large-scale structure of Universe.

1 INTRODUCTION

An important means of determining and/or constraining cosmological parameters is to compare the growth of structure as predicted by theoretical models with that observed in the actual universe. The complexity and sophistication of theoretical approaches span an enormous range of possibilities. Linear perturbation theory provides the simplest analytic description of growth, generally suitable when the perturbation expansion parameter is small. Quasi-linear theory extends the accuracy and applicability of the description at the cost of increasingly complex formulations. Finally, an N-body simulation is capable of handling fully non-linear situations and delivering, in principle, exact answers albeit at substantial computational cost and without the benefit of analytic insight. The choice of a particular method is best determined by the sort of problem one intends to solve. For example, if one is interested in calculating how an initial Gaussian perturbation spectrum generates non-Gaussianity as structure forms then one seeks an accurate method for treating perturbations once mode-mode coupling becomes important. As in Goldilocks’s fable the extreme choices may prove unpalatable: on the one hand, the coupling of interest is absent in a purely linear analysis; on the other, particle-based methodologies introduce spurious shot noise

* E-mail: sharvari@iitk.ac.in

† E-mail: chernoff@astro.cornell.edu

in representations of the underlying smooth density distribution so that high accuracy may demand infeasible numbers of particles.

This paper’s focus is the development of a middle approach, a method for the numerical treatment of structure formation based on intrinsically smooth descriptions of the density and velocity fields and capable of tracing quasi-linear evolution to arbitrary accuracy. We anticipate it will find application in situations where small non-linear effects and/or highly accurate results prior to collapse are of primary interest. The physical context is Newtonian cosmology i.e. sub-horizon scales, non-relativistic velocities and weak gravitational fields. The methods are applicable until the formation of the first caustic. Future studies will extend the methodology to reach beyond particle crossing and to handle physical scales approaching that of the horizon.

Lagrangian perturbation theory (LPT), the heart of the approach employed here, has been well-studied. Lagrange variables in the context of gravity were introduced more than four decades ago (Novikov 1969). Its use in cosmology was initiated by Zel’dovich who gave an approximate analytic solution for special initial conditions with peculiar velocity proportional to peculiar acceleration (Zel’dovich 1970). This is the famous “Zel’dovich approximation” for the evolution of growing modes where “approximate” means accurate to first order in particle displacements. Buchert’s studies (Buchert 1989; Buchert 1992, henceforth B92) enlarged the class of initial conditions that could be solved to first-order. Generalizations of the equations of motion, the initial conditions, the perturbation order and the method of solution have appeared regularly (Moutarde et al. 1991; Bouchet et al. 1992; Buchert & Ehlers 1993, henceforth BE93; Buchert 1994, henceforth B94; Catelan 1995; Munshi, Sahni, & Starobinsky 1994; Bouchet et al. 1995; Ehlers & Buchert 1997, henceforth EB97; Rampf & Buchert 2012; Rampf & Rigopoulos 2012; Rampf & Wong 2012; Rampf 2012; Tatekawa 2012). Physical extensions include general relativistic equations of motion (Kasai 1995) and the treatment of relativistic fluids (Matarrese & Terranova 1996; Matarrese, Pantano, & Saez 1993, 1994).

LPT has proven to be a practical tool in many different applications including modelling the non-linear halo mass functions (Monaco 1997; Monaco, Theuns, & Taffoni 2002; Scoccimarro & Sheth 2002), reconstructing baryon acoustic oscillations (Eisenstein et al. 2007), modelling the non-linear density velocity relation (Kitaura et al. 2012) and setting up the initial conditions for fully numerical simulations (Scoccimarro 1998; Crocce, Pueblas, & Scoccimarro 2006).

An assumption common to all these treatments is that the matter velocity at a point in space is single valued (the distribution is “cold”). LPT breaks down once particle orbits begin to cross, caustics appear, densities diverge and physical singularities first form. Nothing in this paper ameliorates the onset of these effects. There have been interesting suggestions on how one might modify LPT to handle this fundamental limitation (e.g. Adler & Buchert 1999) but we do not pursue the issue here. For our purposes the immediate concern is a new limitation of LPT that has recently come to light. The convergence of the formal series expansion which is the basis of LPT turns out to be limited in time (Nadkarni-Ghosh & Chernoff 2011, hereafter NC11). No one would be surprised that the onset of particle crossings inhibits the utility of the formal perturbation expansion for subsequent times. What was unexpected and striking to us was the existence of limits in a variety of other situations, even cosmologies lacking future particle crossings and devoid of future physical singularities. To the best of our knowledge Sahni & Shandarin (1996) were the first to report the failure of LPT to describe one of the simplest cosmological problems, the evolution of spherical homogeneous voids. We confirmed their result, investigated the issue for all top-hat cosmologies and traced the problem to the occurrence of poles in a suitable set of analytically continued equations of motion. We complemented this mathematical explanation with direct numerical evaluation of the LPT series in all qualitatively distinct regimes for top-hat like cosmologies. The upshot is the existence of a non-trivial limit to the future times for which the LPT description converges. We dubbed the interval when convergence of the perturbation expansion occurs as the “time of validity.” Even if one could work to infinite order in the perturbation amplitude the LPT series would fail to give the correct answer at times outside the interval. The end of the time of validity *precedes* any limitation due to particle crossing. Figure 1 shows the first 15 orders of the LPT description for a simple underdense top-hat. The time of validity extends only up until $a \sim 0.2$.

Like us many readers may find it odd that this behaviour had not been previously reported in a model as well-studied as the top-hat but we can point to two reasons. First, convergence of LPT had never been addressed in a systematic fashion. Second, for collapsing Zel’dovich initial conditions (initial velocity and acceleration proportional) the situation is degenerate in the following sense: the convergence limitations become identical to the moment of caustic formation. Generically, however, the time of validity for top-hat evolution does not extend up to the first particle crossings and is the more stringent restriction. To calculate the “answer” beyond the time of validity we proposed to evaluate the solution at an intermediate time when the series is still valid and use the results as initial conditions for a new expansion about the intermediate point. We worked out the details for this solution technique which we dubbed “LPT re-expansion”. It is roughly analogous to analytic continuation of a power series in the complex plane. Re-expansion will not circumvent the ultimate limitation set by particle crossing but it will allow the solution to be extended to this maximum possible future time after which the flow is no longer cold. We provided detailed numerical examples of how LPT re-expansion handles the previous difficulties encountered in the top-hat problem.

Although our analysis was specific to one of the simplest of all cosmological problems we believe these ideas are valid

in more general circumstances. Consequently, one should shift from thinking of LPT as a one step, stand-alone method of calculation to viewing it as the fundamental operation in a numerical, multi-step method of solution. Our development of LPT re-expansion resembles a traditional finite-difference method in that the system is updated on a step-by-step basis. Just as is true for particle-based calculations, stability limits how big a step can be taken and accuracy varies with step size and expansion order.

This paper works out LPT with re-expansion for general inhomogeneous initial conditions in a flat Friedmann-Robertson-Walker (FRW) background cosmology. We present fundamental mathematical results, practical computational methods and stringent numerical tests. This paper serves as a ‘proof of principle’ demonstration of the method. We will provide practical cosmological applications in subsequent papers.

In §2 we describe the Lagrangian framework and the relationship of the full solution of the geodesic equation of motion for particles to that provided by the LPT expansion. The formal expression for the latter is derived by first taking spatial derivatives of the geodesic equation (B92; BE93; B94; EB97). This system is invariant under spatially uniform, time-dependent translations. As we show in some detail, it is necessary to fix this degree of freedom to recover the physical solution. This involves supplementing the order-by-order LPT solution with purely temporal functions, which we refer to as ‘frame shifts’. This issue has never been addressed for single-step applications of LPT. For some initial conditions the omission turns out to be inconsequential but for most others it breaks momentum conservation. Moreover, when multiple steps are taken it becomes crucial to employ the full solution at each stage of the calculation. We will show that the numerical method converges if and only if that is done.

This paper notably differs from most previous approaches by considering initial conditions of a completely general nature. LPT is often used to propagate the small fluctuations present at recombination to a modest redshift for the purpose of initialising an N-body treatment. In studies of cosmological structure formation it is common to begin from Zel’dovich initial conditions since vorticity modes decay away in an expanding universe. The damping is normally sufficient to obviate the influence of the initial vorticity so that an LPT treatment of the growing modes alone is adequate for setting up an N-body treatment of structure formation in pure Λ CDM. Vorticity is intrinsically generated once non-linearities form and particle crossing begins; these complications are accurately handled by traditional N-body methods. In this context, there is little need for treating arbitrary initial data.

Of course having a capability to study both longitudinal and transverse motions opens up interesting possibilities involving additional participants in structure formation such as magnetic fields and cosmic strings since these may act to introduce vorticity into the cosmic flows at late times. But the main motivation to work in full generality is to facilitate the use of LPT as part of a future calculational approach meant to treat non-linear structure formation. In any realistic multi-step numerical approach (analogous to that developed herein) vorticity will inevitably appear just as it does in traditional N-body treatments. After it arises each step of a multi-step calculation must be able to handle essentially arbitrary density and velocity configurations as initial data. The ability to treat these initial conditions with LPT is a pre-requisite for utilizing LPT itself in the future approach. That is the main reason we work in full generality.

§2 includes an outline of the design and implementation of the re-expansion algorithm. §3 summarizes tests for both special and general initial conditions. We test the algorithm’s ability to reproduce known solutions. We analyse the dependence of errors on Lagrangian order, step size and size of the numerical grid. Taken together these tests validate the concept of Lagrangian re-expansion, its analytic form and our computational implementation. All tests are for small grid sizes but we expect the methods demonstrated to apply without essential modification to larger scale calculations.

§4 presents conclusions and possible future developments.

2 GRAVITATIONAL FIELD EQUATIONS IN THE LAGRANGIAN FRAMEWORK

2.1 General Setup

Assume a flat FRW background cosmology with scale factor $a(t)$ that contains pressureless dark matter with average density $\rho_m(t)$ and time-dependent dark energy with average density $\rho_X(t)$ having fixed equation of state parameter w . We do not distinguish between cold baryons and cold collisionless matter and we work before the formation of caustics. The homogeneous background evolution is determined by the initial scale factor a_0 , Hubble constant H_0 and matter and dark energy densities, $\rho_{m,0}$ and $\rho_{X,0}$ respectively. The subscript “0” indicates time t_0 which may differ from the current epoch.

We intend that the initial conditions allow for arbitrary density and velocity perturbations of cold dark matter subject to minimal restrictions. We constrain the dark energy component to be spatially uniform at all times¹. We work in an expanding, periodic volume, a 3-torus. For physical, cosmological applications this volume is intended to be (1) a fair representation of

¹ Although it has been suggested that quintessence models with $w \neq -1$ should have spatial fluctuations (for example Caldwell, Dave, & Steinhardt 1997), these fluctuations are estimated to be small (for example Mota, Shaw, & Silk 2008; Cooray, Holz, & Caldwell 2010).

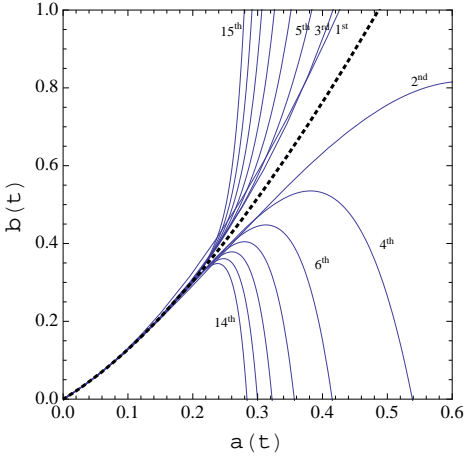


Figure 1. Convergence of LPT: $a(t)$ and $b(t)$ are the scale factors of the background and the underdense spherical perturbation, respectively. The black dotted line is the exact open model with $\delta\rho/\rho = -9 \times 10^{-3}$ at $a = 10^{-3}$ and fractional Hubble velocity 3×10^{-3} . The blue lines show successive higher order approximations from 1 to 15 (as labeled). The LPT series converges only $a \lesssim 0.2$ even though there is no future singularity in this cosmology. LPT re-expansion provides a method to extend the solution to arbitrarily large a in this example.

the actual universe and (2) one that can be accurately treated in the Newtonian limit. Our perturbative approach does not allow any back-reaction of the small-scale physics on the large-scale expansion of the homogeneous and isotropic background. Consistency requires that the initial mean density of the inhomogeneous matter distribution agree exactly with that of the background cosmology. Mathematically, the evolution of the inhomogeneous Newtonian problem is completely determined by the otherwise arbitrary, initial density and velocity perturbations. We must check, in principle, that the Newtonian limit is valid at all times.

2.2 Lagrangian Picture

We will start by assuming that the coordinate system of the periodic volume coincides with one of the family of preferred world lines in FRW cosmology, i.e. one for which the CMB dipole vanishes. We will refer to this starting point as the OBS “inertial frame” and the observers as “inertial observers”.

In the Lagrangian picture the particle position is a function of time and a set of Lagrangian labels \mathbf{Y} . The labels are assigned at the initial time and, for our purposes, are always taken to be initial comoving Eulerian positions. We write $\mathbf{x}(t; \mathbf{Y})$ for the instantaneous comoving coordinate of a fluid particle. By contrast, in the Eulerian picture \mathbf{x} is an independent variable that identifies a fixed grid position. For notational simplicity we will often use the descriptive shorthand that \mathbf{x} is either Lagrangian (equivalently, a particle) or Eulerian.

In many applications one starts with a finite, discrete set of particles (e.g. an N-body code) but here we assume space is completely filled with particles. In effect, we promote the discrete set of Lagrangian labels to a continuous field throughout space so that at any time it is possible to relate an Eulerian grid coordinate to a Lagrangian label in a one-to-one fashion. Mathematically, the existence of a well-defined velocity field at every point in space establishes this result (EB97). The Lagrangian particle velocity is identical to the Eulerian velocity at the grid position that coincides with the particle position.

Throughout this paper we will use the following convention for density: $\rho(\mathbf{r}, t)$ is the physical density expressed as a function of \mathbf{r} , the physical position, and $\rho(\mathbf{x}, t)$ is the same numerical quantity expressed as a function of \mathbf{x} , the comoving coordinate. Explicitly, we have

$$\rho(\mathbf{x}, t) \equiv \rho(\mathbf{r}, t)|_{\mathbf{r}=\mathbf{a}\mathbf{x}} \quad (1)$$

$$\Delta M = \rho(\mathbf{r}, t)d^3r = \rho(\mathbf{x}, t)d^3r = \rho(\mathbf{x}, t)a^3d^3x. \quad (2)$$

Note that $\rho(\mathbf{x}, t)$ is *not* the comoving density.

Likewise, we employ a similar convention for density written in terms of the Lagrangian variable

$$\rho(\mathbf{Y}, t) \equiv \rho(\mathbf{r}, t)|_{\mathbf{r}=\mathbf{r}(\mathbf{Y}, t)} \quad (3)$$

$$\Delta M = \rho(\mathbf{r}, t)d^3r = \rho(\mathbf{Y}, t)d^3r = \rho(\mathbf{Y}, t)J(\mathbf{Y}, t)d^3Y \quad (4)$$

$$J(\mathbf{Y}, t) = \text{Det} \left(\frac{\partial \mathbf{r}}{\partial \mathbf{Y}} \right) \quad (5)$$

where $\mathbf{r}(\mathbf{Y}, t)$ is the physical position of the particle labeled by Lagrangian coordinate \mathbf{Y} and J is the determinant of the

coordinate transformation. The distinguishing feature of the Lagrangian labels is that they track the mass so, in addition to the above general properties, we also have mass conservation in the form

$$\rho(\mathbf{Y}, t)J(\mathbf{Y}, t) = \rho(\mathbf{Y}, t')J(\mathbf{Y}, t') \quad (6)$$

for any times t and t' .

In comoving coordinates the Newtonian limit of the geodesic equation and of Poisson's equation for the gravitational potential $\psi(\mathbf{x}, t)$ are

$$\frac{d}{dt} \left(a^2 \frac{d\mathbf{x}}{dt} \right) = -\nabla_x \psi(\mathbf{x}, t) \quad (7)$$

$$\nabla_x^2 \psi(\mathbf{x}, t) = 4\pi G a^2 \delta\rho_m(\mathbf{x}, t) \quad (8)$$

where $a(t)$ is the scale factor and $\delta\rho_m(\mathbf{x}, t)$ is the physical matter density perturbation. There is also an equation for mass conservation. The x -related terms are Eulerian except for those on the left-hand side of the first equation which refer to particles (d/dt and \mathbf{x}). The time-derivative is the 'Lagrangian' or 'convective' derivative,

$$\frac{d}{dt} = \frac{\partial}{\partial t} + \mathbf{v} \cdot \nabla_x, \quad (9)$$

where \mathbf{v} is the Eulerian velocity. The operator commutes with the Lagrangian spatial derivative but not the Eulerian one.

To make mathematical sense of these equations as a Lagrangian system we should, schematically, specify Lagrangian labels at the initial time and transform the Eulerian to Lagrangian forms while imposing the condition that the Eulerian coordinate match the particle position.

We regard the system as posing an initial value problem for the particle positions and velocities. If the initial conditions are specified as Eulerian density and velocity perturbations then they must be transformed to particle positions and velocities. The density perturbation is a functional of the initial density and the initial and final particle positions. The potential can be solved at any time the density is known.

In physical coordinates $\mathbf{r} = a(t)\mathbf{x}$ we have

$$a\ddot{\mathbf{r}} - \dot{a}\dot{\mathbf{r}} = -a\nabla_r \psi(\mathbf{r}, t) \quad (10)$$

$$\nabla_r^2 \psi(\mathbf{r}, t) = 4\pi G \delta\rho_m(\mathbf{r}, t), \quad (11)$$

where the dot denotes the total derivative with respect to time. As above, $\mathbf{r}(t)$ and $\ddot{\mathbf{r}}(t)$ (left-hand side of the first equation) refers to particles while the structure of the remaining terms is Eulerian.

Buchert and Ehlers' derivation of the Lagrangian equations of motion (B92, BE93, B94, EB97) involves taking the Eulerian divergence and curl of the first equation, combining with the second and using the homogeneous equations for the scale factor $a(t)$ to give

$$\nabla_r \cdot \ddot{\mathbf{r}} = -4\pi G [\rho_m(\mathbf{r}, t) + \rho_X(t)(1 + 3w)] \quad (12)$$

$$\nabla_r \times \ddot{\mathbf{r}} = 0, \quad (13)$$

where $\rho_m(\mathbf{r}, t)$ and $\rho_X(t)$ are the matter and dark energy densities respectively. These steps can eliminate the potential and operator occurrences of \mathbf{x} or \mathbf{r} on the right-hand side. The essential complication, however, is that the derivative form of the geodesic equations is insensitive to a spatially homogeneous arbitrary, time-dependent vector shift $\Delta\mathbf{r}(t)$.

The solution of the resultant Lagrangian system by Ehlers and Buchert (EB97) is achieved in a specific frame, one in which the initial, spatially averaged peculiar velocity vanishes. We must address the relationship between the solutions of the geodesic equation and of this specific solution of the derivative form of the geodesic equation. To handle this situation carefully, we start in the observer frame (denoted by OBS) and introduce the Ehlers-Buchert frame (denoted by EB). The solution to the geodesic equation lies in the former and the specific solution to the derivative form in the latter. The connection is called the frame shift.

Schematically, the initial data is specified in the OBS frame, transformed to the EB frame, solved in the EB frame using EB's perturbative expansion and then transformed back to the OBS frame. The EB frame is not an inertial frame and the transformation between the two frames is not a Galilean transformation. We regard the EB frame as a computational frame; it coincides with the physical observer frame only at the initial time.

2.3 Notation for Observer and EB Frames

Begin by assuming that each frame possesses its own comoving coordinate system. Imagine a single particle variously described according to multiple coordinate systems. In each frame the Lagrangian label is assigned to be the comoving Eulerian coordinate at the initial time

$$\mathbf{Y} = \mathbf{x}_{OBS,0} \quad (14)$$

$$\mathbf{X} = \mathbf{x}_{EB,0}. \quad (15)$$

At future times the particles positions are written $\mathbf{x}_{OBS}(\mathbf{Y}, t)$ and $\mathbf{x}_{EB}(\mathbf{X}, t)$, respectively. Physical coordinates, Jacobians relating Eulerian to Lagrangian coordinates and volume elements are defined in the usual manner in the OBS frame

$$\mathbf{r}_{OBS}(\mathbf{Y}, t) = a(t)\mathbf{x}_{OBS}(\mathbf{Y}, t) \quad (16)$$

$$J(\mathbf{Y}, t) = \text{Det} \left(\frac{\partial \mathbf{r}_{OBS}}{\partial \mathbf{Y}} \right) \quad (17)$$

$$d^3 x_{OBS} = \frac{J(\mathbf{Y}, t)}{a^3} d^3 Y \quad (18)$$

and it follows $J(\mathbf{Y}, t_0) = a_0^3$. Similar definitions are given in the EB frame.

Without loss of generality choose the two frames to coincide at the initial time, $\mathbf{x}_{OBS} = \mathbf{x}_{EB}$ and $\mathbf{Y} = \mathbf{X}$, and write the relationship between the comoving coordinates as a pure function of time

$$\mathbf{x}_{OBS}(\mathbf{Y}, t) = \mathbf{x}_{EB}(\mathbf{X}, t) + \Delta \mathbf{x}(t). \quad (19)$$

Here, $\Delta \mathbf{x}(t)$ is the comoving frame shift. Next, define $\Delta \mathbf{r}$ in terms of $\Delta \mathbf{x}$

$$\Delta \mathbf{r}(t) = a(t)\Delta \mathbf{x}(t). \quad (20)$$

We now have

$$\Delta \mathbf{x}(t_0) = \Delta \mathbf{r}(t_0) = 0 \quad (21)$$

$$J(\mathbf{Y}, t) = J(\mathbf{X}, t). \quad (22)$$

Initially, $d^3 x_{OBS} = d^3 Y = d^3 X = d^3 x_{EB}$, and at all times the Eulerian volume elements satisfy $d^3 x_{OBS} = d^3 x_{EB}$ and the Lagrangian volume elements $d^3 Y = d^3 X$. We will choose $\dot{\Delta} \mathbf{x}(t_0)$ in a moment and then later make use of the remaining freedom to choose $\Delta \mathbf{x}(t)$ so that the geodesic equation is solved.

The physical mass density is $\rho_m(\mathbf{r}, t)$. Since it's a scalar it remains unchanged by the EB to OBS transformation. Mass conservation and equations (6) and (18) give

$$\rho_m(\mathbf{x}, t) a^3 d^3 x_{OBS} = \rho_m(\mathbf{Y}, t_0) a_0^3 d^3 Y. \quad (23)$$

The peculiar velocity is defined

$$\mathbf{v}_{OBS}(\mathbf{Y}, t) = \dot{\mathbf{r}}_{OBS}(\mathbf{Y}, t) - \frac{\dot{a}}{a} \mathbf{r}_{OBS}(\mathbf{Y}, t) \quad (24)$$

$$= a \dot{\mathbf{x}}_{OBS}(\mathbf{Y}, t) \quad (25)$$

and likewise for \mathbf{v}_{EB} . The peculiar velocity shift is defined

$$\Delta \mathbf{v}(t) = \mathbf{v}_{OBS}(\mathbf{Y}, t) - \mathbf{v}_{EB}(\mathbf{X}, t) \quad (26)$$

$$= \dot{\Delta} \mathbf{r}(t) - \frac{\dot{a}}{a} \Delta \mathbf{r}(t) \quad (27)$$

$$= a \dot{\Delta} \mathbf{x}(t). \quad (28)$$

2.4 Transformation from Observer to EB Frame

The perturbation is characterized by two quantities specified in the observer frame; the initial fractional overdensity

$$\delta_{OBS}(\mathbf{Y}, t_0) = \frac{\rho_m(\mathbf{Y}, t_0)}{\rho_{m,0}} - 1 \quad (29)$$

and the initial peculiar velocity

$$\mathbf{v}_{OBS}(\mathbf{Y}, t_0) = \dot{\mathbf{r}}_{OBS}(\mathbf{Y}, t_0) - \dot{a}_0 \mathbf{Y}. \quad (30)$$

The density perturbation is a scalar quantity so transferring to the EB frame is immediate

$$\delta_{EB}(\mathbf{X}, t_0) = \delta_{OBS}(\mathbf{Y}, t_0) \quad (31)$$

and we will henceforth drop the ‘‘subscript’’ that distinguishes these two.

The initial peculiar velocity is a vector quantity which transforms like

$$\mathbf{v}_{EB}(\mathbf{X}, t_0) = \mathbf{v}_{OBS}(\mathbf{Y}, t_0) - \mathbf{v}_{c,0} \quad (32)$$

where $\mathbf{v}_{c,0}$ is a constant we will now choose. Let $\langle \dots \rangle_s \equiv (\int d^3 s \dots) / \int d^3 s$ denote the average of a quantity over the variable ‘‘s’’. In this notation, the average peculiar velocity in the OBS frame at *any time* t is

$$\mathbf{v}_c(t) = \langle \mathbf{v}_{OBS}(\mathbf{x}_{OBS}, t) \rangle_{\mathbf{x}_{OBS}}. \quad (33)$$

We want to ensure that the average peculiar velocity in the EB frame vanishes at the beginning of the step, $\langle \mathbf{v}_{EB} \rangle_X = 0$, as assumed in the formal perturbative scheme given in EB97 (see §2.6).

From equation (32), this requirement sets $\Delta \mathbf{v}(t_0) = \mathbf{v}_{c,0} = \mathbf{v}_c(t_0)$. At the beginning of the step the Eulerian and Lagrangian coordinate systems coincide, $\Delta \mathbf{r}(t_0) = 0$, and the initial time derivative of the frame shift is

$$\dot{\Delta} \mathbf{r}(t_0) = a_0 \dot{\Delta} \mathbf{x}(t_0) = \mathbf{v}_{c,0}. \quad (34)$$

Equation (32) refers to the initial condition whereas equation (26) applies at all times during a step. In §2.7 we give explicit expression for the shift accumulated during a time t . If one takes a single step then $\mathbf{v}_{c,0}$ is computed once at the start of the evolution. At the end of the step accumulated position and velocity shifts are added to the EB frame results to obtain the solution in the OBS frame. If one re-expands the solution, one takes multiple steps and repeats the process over and over.

2.5 Equations in EB Frame

Conservation of mass and equations (15), (29) and (31) imply

$$\delta(\mathbf{X}, t) = \frac{(1 + \delta(\mathbf{X}, t_0))a^3}{J(\mathbf{X}, t)} - 1. \quad (35)$$

The density evolution of dark energy (denoted by a subscript X not to be confused with the Lagrangian coordinate) for a constant equation of state w is

$$\rho_X(t) = \rho_{X,0} \left(\frac{a_0}{a} \right)^{3(1+w)}. \quad (36)$$

These allow one to express the right-hand side of equation (12) in terms of Lagrangian coordinates. We transform all the derivatives with respect to the Eulerian coordinates $\mathbf{r} \equiv \mathbf{r}_{EB}$ in equation (12) and (13) to derivatives with respect to the Lagrangian coordinates (Appendix A furnishes additional details). The complete set of equations is

$$\begin{aligned} \hat{L}[\ddot{\mathbf{r}}_{EB}, \mathbf{r}_{EB}, \mathbf{r}_{EB}] &= -3H_0^2 \Omega_{m,0} a_0^3 (1 + \delta(\mathbf{X}, t_0)) \\ &\quad - \frac{H_0^2}{2} (1 + 3w) \Omega_{X,0} \left(\frac{a_0}{a} \right)^{3(1+w)} \hat{L}[\mathbf{r}_{EB}, \mathbf{r}_{EB}, \mathbf{r}_{EB}], \end{aligned} \quad (37)$$

$$\hat{\mathbf{T}}[\ddot{\mathbf{r}}_{EB}, \mathbf{r}_{EB}] = 0, \quad (38)$$

where

$$\Omega_{m,0} = \frac{8\pi G \rho_{m,0}}{3H_0^2}, \quad (39)$$

$$\Omega_{X,0} = \frac{8\pi G \rho_{X,0}}{3H_0^2} \quad (40)$$

and the action of \hat{L} and $\hat{\mathbf{T}}$ operators on general vectors $\mathbf{A}, \mathbf{B}, \mathbf{C}$ is defined as

$$\hat{L}[\mathbf{A}, \mathbf{B}, \mathbf{C}] = \epsilon_{lmq} \epsilon_{ijk} \frac{\partial A_i}{\partial X_l} \frac{\partial B_j}{\partial X_m} \frac{\partial C_k}{\partial X_q}, \quad (41)$$

$$\hat{\mathbf{T}}_q[\mathbf{A}, \mathbf{B}] = \epsilon_{lmq} \frac{\partial A_k}{\partial X_l} \frac{\partial B_k}{\partial X_m}. \quad (42)$$

Here ϵ_{ijk} is the usual Levi-Civita symbol and Einstein's summation convention is used. The scalar operator \hat{L} and vector operator $\hat{\mathbf{T}}$ provide a compact representation.

The specification of $a_0, H_0, \Omega_{m,0}, \Omega_{X,0}, w$, the initial fractional overdensity and the initial peculiar velocity determines the solution. The fractional overdensity appears explicitly in the equations above; the peculiar velocity enters as initial conditions for $\dot{\mathbf{r}}_{EB}$. The system defined by equations (37) and (38) can be found in EB97 (see references therein for prior versions) for the case of a cosmological constant. The generalization here allows for time-dependent dark energy term.

2.6 EB Perturbation scheme

In the formalism outlined by B92, BE93, B94 and EB97, the physical coordinate is split

$$\mathbf{r}_{EB}(\mathbf{X}, t) = a(t)\mathbf{X} + \mathbf{p}(\mathbf{X}, t) \quad (43)$$

where the first term is the position in a homogeneous universe (zero density perturbations and zero peculiar velocities) and the second represents displacements that occur in the general case. The choice of the initial comoving coordinate as the Lagrangian label (equation 15) implies $\mathbf{p}(\mathbf{X}, t_0) = 0$.

The displacement vector is expanded

$$\mathbf{r}_{EB}(\mathbf{X}, t) = a(t)\mathbf{X} + \sum_{n=1} \mathbf{p}^{(n)}(\mathbf{X}, t)\epsilon^n, \quad (44)$$

where ϵ is the formal, bookkeeping device that tracks the order of the displacement. Substitute the ansatz equation (44) into equations (37) and (38) and equate the terms of the same order of ϵ to generate a hierarchy of equations to be solved. Since the Lagrangian labelling is independent of time the derivatives of interest commute: $[d/dt, \nabla_{\mathbf{X}}] = 0$. This makes it straightforward to find $\dot{\mathbf{r}}_{EB}$ and $\ddot{\mathbf{r}}_{EB}$.

This formal treatment at *zeroth order* of equation (37) reduces to

$$\frac{\ddot{a}}{a} = -\frac{H_0^2}{2} \left(\frac{\Omega_{m,0} a_0^3}{a^3} + (1+3w)\Omega_{X,0} \left(\frac{a_0}{a} \right)^{3(1+w)} \right) \quad (45)$$

while equation (38) is identically zero. This is simply the equation governing the background scale factor. Given $a_0, H_0, \Omega_{m,0}, \Omega_{X,0}$ and w the background evolution is completely determined.

At first order equations (37) and (38) reduce to

$$D_t^L [\nabla_{\mathbf{X}} \cdot \mathbf{p}^{(1)}] = -\frac{3}{2} H_0^2 \Omega_{m,0} a_0^3 \delta(\mathbf{X}, t_0) \quad (46)$$

$$D_t^T [\nabla_{\mathbf{X}} \times \mathbf{p}^{(1)}] = 0 \quad (47)$$

and at higher orders to

$$D_t^L [\nabla_{\mathbf{X}} \cdot \mathbf{p}^{(n)}] = S^{(n,L)} \quad (48)$$

$$D_t^T [\nabla_{\mathbf{X}} \times \mathbf{p}^{(n)}] = \mathbf{S}^{(n,T)}, \quad (49)$$

where the operators are

$$D_t^L = \left(2a\ddot{a} + \frac{3}{2} a^2 H_0^2 (1+3w)\Omega_{X,0} \left(\frac{a_0}{a} \right)^{3(1+w)} + a^2 \frac{d^2}{dt^2} \right), \quad (50)$$

$$D_t^T = \left(-\ddot{a} + a \frac{d^2}{dt^2} \right) \quad (51)$$

and $S^{(n,L)}$ and $\mathbf{S}^{(n,T)}$ are scalar and vector source terms comprised of combinations of displacements with order $< n$. An explicit form is given in the Appendix B. Here L and T refer to longitudinal and transverse operators.

Next, the displacement is split into longitudinal and transverse parts, order-by-order:

$$\mathbf{p}^{(n)} = \mathbf{p}^{(n,L)} + \mathbf{p}^{(n,T)}, \quad (52)$$

where $\nabla_{\mathbf{X}} \times \mathbf{p}^{(n,L)} = 0$ and $\nabla_{\mathbf{X}} \cdot \mathbf{p}^{(n,T)} = 0$. On the 3-torus, a unique decomposition for order n requires $\langle \mathbf{p}^{(n)}(\mathbf{X}, t) \rangle_{\mathbf{X}} = 0$ (see Appendix C of EB97 for the mathematical proof). The choice of Lagrangian labels guarantees the condition is satisfied at $t = t_0$ for all n . If the volume-averaged source terms vanish at all times then the decomposition is also possible at future times. Appendix C shows that $\langle \mathbf{p}^{(1)}(\mathbf{X}, t) \rangle_{\mathbf{X}} = 0$ at future times if both the overdensity and the peculiar velocity average to zero *initially*, which is the case (the latter by the choice of the EB frame). Using the $n = 1$ results one next shows that the average scalar and vector source terms for $n = 2$ displacements vanish so $\langle \mathbf{p}^{(2)}(\mathbf{X}, t) \rangle_{\mathbf{X}} = 0$ and this argument is extended order-by-order. The result is that the requirements for decomposition are satisfied at all orders.

Separating longitudinal and transverse displacements order-by-order uncouples the left-hand sides of equations (48) and (49) and rationalizes the ‘‘L’’ and ‘‘T’’ labelling *a posteriori*. There are separate source term ($S^{(n,L)}, \mathbf{S}^{(n,T)}$) but note that each depends upon both types of lower order solutions ($\mathbf{p}^{(m,L)}$ and $\mathbf{p}^{(m,T)}$ for $m < n$). The entire solution at lower orders is needed to compute either the longitudinal or transverse source for a given order.

The specification of the initial conditions for the hierarchy of equations determines the physical meaning of the formal perturbative expansion in powers of ϵ . We make specific choices to ensure that the initial density and velocity perturbations are first order in ϵ . The first choice is $\mathbf{p}^{(n,L/T)}(\mathbf{X}, t_0) = 0$ for all n (‘‘L/T’’ means the equation applies to both longitudinal and transverse displacements) which is sufficient but not necessary to insure zero initial displacement. Homogeneous initial data makes it easy to use the formal structure of the hierarchy to check how powers of density and velocity enter. The density appears explicitly only at first order, i.e. in the equation for $\mathbf{p}^{(1,L)}$. The second choice is that the peculiar velocity is assigned as initial data only to the derivative of the first order term

$$\dot{\mathbf{p}}^{(1,L/T)}(\mathbf{X}, t_0) = \mathbf{v}_{EB}^{L/T}(\mathbf{X}, t_0) \quad (53)$$

where $\mathbf{v}_{EB}^{L/T}(\mathbf{X}, t_0)$ are the curl-free and divergence-less parts of the initial velocity. For all $n > 1$

$$\dot{\mathbf{p}}^{(n,L/T)}(\mathbf{X}, t_0) = 0. \quad (54)$$

One might contemplate other choices (i.e., one could deviate from homogeneous for the displacements and/or distribute the peculiar velocity to different orders) but these would not have the simple physical interpretation that the natural choices provide and could vitiate the split into longitudinal and transverse components.

In equations (46), (47), (48) and (49) the spatial and temporal operators commute and the spatial and temporal parts of the solution decouple at each order (see Appendix B). The solution is a sum of spatial parts times temporal parts. Each spatial part involves solving linear, elliptic partial differential equations of the form $\nabla \cdot \mathbf{F} = S^L$ or $\nabla \times \mathbf{F} = \mathbf{S}^T$ with known sources S^L , \mathbf{S}^T (Poisson-like problems). Each temporal part involves solving a second order ordinary differential equation in time (initial value problems). Both sets of equations include coefficients that depend upon the background cosmology.

As a practical matter all the Poisson-like equations are solved using Fourier transforms on a $N \times N \times N$ grid with equally spaced grid points which represent the Lagrangian coordinates. Initial value equations are solved numerically using a standard differential equation solver. The individual displacement terms are summed to reconstruct $\mathbf{r}_{EB}(\mathbf{X}, t)$ using equation (44).

2.7 Frame shifts

The LPT expansion described in the previous section yields the position, velocity and density in the EB frame. To get the corresponding answers in the observer frame one must add the time dependent frame shifts (equations 19 and 26).

Start with the Newtonian limit of the geodesic equation in the observer frame

$$\frac{d}{dt} \left(a^2 \frac{d\mathbf{x}_{OBS}}{dt} \right) = -\nabla_{\mathbf{x}_{OBS}} \psi(\mathbf{x}_{OBS}, t) \quad (55)$$

and take the average with respect to the Eulerian \mathbf{x}_{OBS} (on the left we would formally replace $d\mathbf{x}_{OBS}/dt$ with the local Eulerian velocity and d/dt with the full convective derivative). The right-hand side is periodic and averages to zero. Now formally we return to the Lagrangian description on the left: substitute for \mathbf{x}_{OBS} from equation (19) and use $d^3x_{OBS} = d^3x_{EB} = J(\mathbf{X}, t)a^{-3}d^3X$ to give

$$\frac{d}{dt} \left(a^2 \frac{d\Delta\mathbf{x}(t)}{dt} \right) = -\frac{1}{V} \int \left[\frac{d}{dt} \left(a^2 \frac{d\mathbf{x}_{EB}}{dt} \right) \right] a^{-3} J(\mathbf{X}, t) d^3X. \quad (56)$$

and $V = \int d^3x$ is the comoving volume of the box (physical volume $a(t)^3V$).

The geodesic equation is satisfied if the shift $\Delta\mathbf{x}$ satisfies this second order ODE with initial conditions $\Delta\mathbf{x}(t_0) = 0$ and $\dot{\Delta}\mathbf{x}(t_0) = \mathbf{v}_{c,0}/a_0$. The solution is

$$\Delta\mathbf{x}(t) = \int_{t_0}^t \left(\frac{1}{a^2} \int_{t_0}^{t'} \mathbf{g}(t'') dt'' \right) dt' + \int_{t_0}^t \frac{\mathbf{v}_{c,0} a_0}{a^2} dt' \quad (57)$$

where

$$\mathbf{g}(t) = -\frac{1}{V} \int \frac{d}{dt} \left(a^2 \dot{\mathbf{x}}_{EB} \right) (a^{-3} J) d^3X \quad (58)$$

$$= -\frac{1}{V} \int (a\ddot{\mathbf{p}} - \ddot{a}\mathbf{p}) (a^{-3} J) d^3X. \quad (59)$$

Note that $\mathbf{g}(t)$ is completely determined from the EB solution.

In the observer's frame the physical position and velocity are

$$\mathbf{r}_{OBS}(\mathbf{Y}, t) = a\mathbf{X} + \mathbf{p}(\mathbf{X}, t) + a\Delta\mathbf{x}(t) \quad (60)$$

$$\dot{\mathbf{r}}_{OBS}(\mathbf{Y}, t) = \dot{a}\mathbf{X} + \dot{\mathbf{p}}(\mathbf{X}, t) + \dot{a}\Delta\mathbf{x}(t) + a\dot{\Delta}\mathbf{x}(t) \quad (61)$$

and hence the peculiar velocity (defined by equation (24)) is

$$\mathbf{v}_{OBS}(\mathbf{Y}, t) = \dot{\mathbf{p}}(\mathbf{X}, t) - \frac{\dot{a}}{a}\mathbf{p}(\mathbf{X}, t) + \frac{\mathbf{v}_{c,0}a_0}{a} + \frac{1}{a} \int_{t_0}^t \mathbf{g}(t') dt'. \quad (62)$$

The density in the observer frame is identical to that in the EB frame

$$\delta_{OBS}(\mathbf{Y}, t) = \delta_{EB}(\mathbf{X}, t) \quad (63)$$

where the right-hand side is given by equation (35).

Note that the frame shift is time-dependent. The right hand side of equation (57) has two integrals: the first arises from requiring that the geodesic equation is satisfied whereas the second is the decay (due to Hubble drag) of the non-zero average initial velocity defined in §2.4. The shift is not a fixed Galilean transformation. It is related to the fact that the system given by equations (12) and (13) is ‘translation covariant’ (Heckmann-Schücking transformation; see Buchert & Götz 1987 and references therein). In particular, the position, velocity *and* acceleration are different in the two frames. The density in

the two frames, as inferred from the divergence of the acceleration, is the same. That operator is insensitive to any time dependent spatially uniform acceleration. Such accelerations are absent in the inertial frame but present in the computational one. Existing treatments of LPT set the frame shift to zero and satisfy equations (12) and (13). However, this does not yield the solution in the OBS frame. We will demonstrate in later sections that ignoring the frame shift destroys momentum conservation and convergence.

2.8 Frame shifts and momentum conservation

Frame shifts ensure that the geodesic equation is properly satisfied. This is not just a mathematical requirement but a physical one. In this section we consider the implications for momentum conservation and drop the explicit OBS subscript for clarity.

The total proper momentum in comoving coordinates written as a sum over mass elements ΔM_i or an integral over Lagrangian labels (i.e. the density at the initial time) is

$$\mathbf{P}(t) = \sum_i a \frac{d\mathbf{x}_i}{dt} \Delta M_i \quad (64)$$

$$= \int a \frac{d\mathbf{x}}{dt} \rho_m(\mathbf{Y}, t_0) a_0^3 d^3 Y. \quad (65)$$

where $x = x(\mathbf{Y}, t)$. Multiply by a and take the time derivative

$$\frac{d(a\mathbf{P})}{dt} = \int \mathbf{Q} \rho_m(\mathbf{Y}, t_0) a_0^3 d^3 Y, \quad (66)$$

$$\mathbf{Q} = \frac{d}{dt} \left(a^2 \frac{d\mathbf{x}}{dt} \right). \quad (67)$$

Now replace the variable of integration \mathbf{Y} with $x = x(\mathbf{Y}, t)$ at the time of interest. This recasts the integration from a Lagrangian to an Eulerian form. Using equation (23) the densities are $\rho_m(\mathbf{Y}, t_0) a_0^3 d^3 Y = \rho_m(\mathbf{x}, t) a^3 d^3 x = (\rho_m(t) + \delta\rho_m(\mathbf{x}, t)) a^3 d^3 x$ and in the last equality we have introduced the background and the fluctuating densities. The integral splits

$$\frac{d(a\mathbf{P})}{dt} = \rho_m(t) a^3 \int \mathbf{Q} d^3 x + a^3 \int \mathbf{Q} \delta\rho_m(\mathbf{x}, t) d^3 x. \quad (68)$$

When the geodesic equation equation (7) is satisfied \mathbf{Q} is proportional to $\nabla\psi$. Since ψ is periodic the first volume integral with integrand proportional to \mathbf{Q} vanishes. When the Poisson equation equation (8) is satisfied one may rewrite $\nabla\psi$ using the formal Green's function for ψ and invoke its symmetries to show that the second integral vanishes. Hence, $d(a\mathbf{P})/dt = 0$ and $\mathbf{P} \propto 1/a$.

If Poisson's equation is solved exactly in the EB frame the second integral will vanish. However, if frame shifts are ignored then the geodesic equation will not be satisfied and the first integral will generally fail to vanish.

A qualitative understanding of why a non-zero \mathbf{v}_c must develop is revealed by looking at a problem with Zel'dovich initial conditions. We characterize this system as starting with first order terms in displacement, peculiar velocity and peculiar acceleration strictly proportional to one and other and negligible higher order terms (see Appendix D for a detailed discussion). Using $\mathbf{v} = a\dot{\mathbf{x}}$, $\rho_m(t) = \rho_{m,0} a_0^3 / a^3$ and the definition of δ , the total momentum is

$$\mathbf{P}(t) = \rho_{m,0} a_0^3 V \left(\mathbf{v}_c(t) + \frac{1}{V} \int \mathbf{v} \delta(\mathbf{x}, t) d^3 x \right) \quad (69)$$

where V is the comoving volume of the box. The initial state with velocity proportional to acceleration implies that the first term $\mathbf{v}_c = 0$ because the system is periodic and the mean acceleration vanishes. The second term $\propto \int \nabla\psi \delta d^3 x = 0$ on account of the symmetries of the Green's function for Poisson's equation. Hence, Zel'dovich initial conditions in a periodic system imply $\mathbf{P}(t_0) = 0$. If/when the system evolves so that \mathbf{v} is no longer proportional to acceleration then the second term will no longer vanish. The first term must be present and non-zero to insure $\mathbf{P}(t) = 0$. In summary, the EB frame's non-zero velocity is intimately tied to the momentum conservation law which is maintained by proper inclusion of the frame shifts.

Whenever a single step, first order scheme is used to initialize an N-body calculation starting with Zel'dovich initial conditions the frame shift vanishes, i.e. $g(t) = 0$, accurate at first order. To see this insert the definition of J from equation (A3), the proportionality of displacement, velocity and acceleration into equation (57). In general, a second order scheme that omits the frame shift completely makes a second order mistake, i.e. is accurate at first order but not second.

This example also helps one understand some special situations when frame shifts are exactly zero. Assume the initial density and velocity field are purely one dimensional i.e., parallel planes of matter in 3D. As long as particle trajectories do not cross the acceleration on a particle is fixed by the initial density field. A single step first order LPT scheme yields an exact description and it is possible to write out explicit expressions for the frame shifts. For this one dimensional limit the mean

velocity (in the OBS comoving coordinate system) is conserved i.e., $\langle \mathbf{v} \rangle_{x_{OBS}} \sim \mathbf{v}_{c,0} a_0 / a$. If it is initially zero, it is always zero. This does *not* imply that frame shifts vanish because there are two contributions, one coming from $\mathbf{v}_{c,0}$ and the other from internal dynamics in equation (57). In one dimension both terms will vanish if the initial velocity is proportional to the initial acceleration. In this special situation the observer and EB frames coincide at all times and the frame shift terms are exactly zero for both single and multi-step schemes. Proofs are provided in Appendix E.

Frame shifts are needed in other contexts and omitting them will generally produce inconsistencies that manifest as lack of momentum conservation. To the best of our knowledge these frame shifts have been ignored in most applications of LPT so far.

Let's briefly consider the physical nature of \mathbf{v}_c . If the box contains a fair sample of the universe and if the comoving coordinate system coincides with the preferred FRW frame (one with an isotropic cosmic microwave background radiation) then one anticipates $\mathbf{v}_{c,0} = 0$. On the other hand, if super-horizon motions are present (so the notion of a fair representation is not satisfied) and/or if the observer's frame is not equivalent to the preferred FRW frame then, generally speaking, $\mathbf{v}_{c,0}$ is non-zero. In such cases the EB frame coincides with the OBS frame only at the beginning of the calculation.

In an inhomogeneous cosmology $\mathbf{v}_c(t)$ is not proportional to the mean momentum in the box. Of course, the box's self-generated gravitational forces cannot impart net momentum to the box as a whole. If the initial net momentum is zero it will always be zero, however, this does *not* imply that \mathbf{v}_c will vanish on future Eulerian comoving grids if it vanishes initially. In particular, if one chooses $\mathbf{v}_c(t_0) = 0$ then at later time t_1 one generally has $\mathbf{v}_c(t_1) \neq 0$.

As a practical matter if one employs the EB method of solution one cannot circumvent the need to start each step by finding the frame where \mathbf{v}_c vanishes. There is no single, adroit selection to be made at the calculation's start because the EB frame is not tied to a conserved quantity.

2.9 LPT re-expansions

The previous two sections describe the complete formalism for single step LPT; start with initial densities and velocities in the OBS frame, transform to the EB frame, solve for the displacements, move back to OBS frame and compute the densities and velocities at the end of the step. Two questions remain. How big a step can be made and what to do if that step doesn't encompass the total evolutionary time of interest?

In NC11 we answered those questions in the context of spherically symmetric perturbations in an $\Omega = 1$ cosmology. We demonstrated that all convergence problems associated with the LPT series could be overcome by re-expanding the series in overlapping time domains with each domain subject to a time of validity criteria. The time of validity was determined rigorously as functions of the initial density and velocity perturbations.

Here, we assume that the time of validity for the inhomogeneous evolution can be estimated by treating each point in the box as if it were an isolated top-hat. That is, we use the local density perturbation and local velocity perturbation to calculate the time interval that would be allowed for a top-hat. We find the maximum time that lies within all the individual intervals throughout the volume and set the time step accordingly.

The fractional overdensity δ and the fractional Hubble parameter δ_v are the specific parameters used to characterize the time of validity for the spherical perturbation. For generic inhomogeneous initial conditions we write the natural generalizations

$$\delta \equiv \delta(\mathbf{Y}, t_0) \tag{70}$$

$$\delta_v \equiv \frac{1}{3H_0} \nabla_{\mathbf{r}} \cdot \dot{\mathbf{r}}(\mathbf{Y}, t_0) - 1 \tag{71}$$

$$= \frac{1}{3\dot{a}_0} \nabla_{\mathbf{Y}} \cdot \mathbf{v}(\mathbf{Y}, t_0). \tag{72}$$

The values for δ and δ_v are identical in OBS and EB frame. The time of validity $T(\delta, \delta_v)$ was determined in NC11; we use those results to find the minimum of T over the Lagrangian grid ².

A positive δ at a point implies an overdense region and a positive δ_v implies an expanding region. From our experience with top-hat evolution we know that if the time of validity is set by an expanding region then the LPT re-expansion scheme has the ability to extend the solution arbitrarily far into the future. If it is set by a collapsing region then the LPT re-expansion can extend the solution to caustic formation. We remind the reader that the re-expansion scheme does not include any physics for treating hot (multi-stream) fluid.

In LPT re-expansion the quantities calculated at the end of one step form initial conditions for the next step. Since each step begins with the Lagrangian coordinates equal to the comoving coordinates there is one additional computation that is necessary. A new Lagrangian coordinate \mathbf{Y}_1 must be defined at the start of the next step; this is related to the Lagrangian coordinate of the previous step \mathbf{Y}_0 by

² The spherical top-hat system has no transverse component so our treatment ignores that additional complication present in the inhomogeneous system. We see no evidence that this omission leads to any practical difficulty in stability or in convergence.

$$\mathbf{Y}_1 = \frac{\mathbf{r}_{OBS}(\mathbf{Y}_0, t_1)}{a(t_1)}, \quad (73)$$

where t_1 is the starting time for the step and $\mathbf{r}_{OBS}(\mathbf{Y}_0, t_1)$ is given by equation (60). The final quantities from the previous step are known on a uniform grid in \mathbf{Y}_0 ; they are transformed so that the initial conditions are specified on a uniform grid in \mathbf{Y}_1 . We solve equation (73) for \mathbf{Y}_0 given uniform \mathbf{Y}_1 and interpolate the final quantities at \mathbf{Y}_1 . We refer to this step as regriding.

As explained in §2.4, $\mathbf{v}_{c,0}$ differs for each step. Utilizing a sequence of frame shifts does not introduce any intrinsic errors. If the calculation were done exactly using infinite order LPT then the frame shifts at the end of a step would be computed exactly and, in turn, would yield the exact solution in the OBS frame. The re-expansion step involves interpolating the final density and velocity in the OBS frame onto a uniform grid. If interpolation were done without error then the new $\mathbf{v}_{c,0}$ at the start of the step would also be exact. In finite accuracy calculations $\mathbf{v}_{c,0}$ is contaminated by errors that are completely analogous to those in density or velocity. The entire solution converges when the tolerances are tightened.

3 NUMERICAL TESTS OF THE CODE

This section checks and verifies the theoretical scheme outlined in §2 by carrying out selective numerical calculations. The truncation error in the calculations depends upon the Lagrangian order (n), the number of time steps (N_t), and the size of the spatial grid (N_s). We will also refer to N_t as the re-expansion frequency.

The basic elements of the calculation are:

- (i) Use FFT (Fast Fourier Transform) methods to solve all spatial equations,
- (ii) Use Runge-kutta integration to solve the ordinary differential equations for the time-dependent coefficients (including the cosmology background),
- (iii) Use Simpson's rule for the quadratures needed to evaluate the frame shifts (eq. (57)),
- (iv) Use Newton's method for root finding and exact periodic interpolation during the regriding step (the most time-consuming task).

Generally, we complete each individual task to machine precision. In the following section “interpolation error” refers to the net total of these four sources of numerical error. The total is typically dominated by the roundoff error in the solution of the spatial equations. These manipulate matrices with $\sim N_s^3$ elements. We observe residual errors at roughly the level $\sim N_s^{3/2} \epsilon_{Machine}$ where $\epsilon_{Machine}$ is the machine precision. The interpolation error is small compared to truncation error in all results we will discuss. The truncation error is the main focus of investigation.

3.1 Convergence and truncation error

Consider evolution over a finite length of time prior to particle crossing in a periodic box of comoving size L . There are two qualitatively distinct LPT schemes that, in principle, are capable of converging to the exact answer:

- (i) Fix N_t and increase n and N_s without bounds.
- (ii) Fix n and increase N_t and N_s without bounds.

In both schemes it is necessary to refine the representation of all spatial functions ($N_s \rightarrow \infty$). In both it is necessary to respect the time of validity for evolution. The first scheme is satisfactory if N_t is sufficiently large; the second scheme which decreases the size of the time steps as $N_t \rightarrow \infty$ will eventually respect *any* non-zero time of validity condition. Hybrid forms in which Lagrangian order and number of steps increase together are also possible.

Achieving a theoretical understanding of the scaling of the errors is important for two reasons. The numerical methods should demonstrate the expected scaling. Agreement between expected and actual scaling is valuable information when one is validating a computer code. In addition, a theoretical understanding helps make the most efficient choices of control parameters for carrying out practical calculations.

In the past, LPT with $N_t = 1$ and fixed n has been applied to practical cosmological problems while the formal convergence issues have generally been ignored. Occasionally, a solution has been studied as a function of the Lagrangian order n for a single step as in the first scheme (Buchert et al. 1997). There are numerous comparisons with N-body calculations (Buchert, Melott, & Weiss 1994, Melott, Buchert, & Weiss 1995, Karakatsanis, Buchert, & Melott 1997) but these are not sufficiently accurate to address the issue of LPT convergence. We will provide a detailed look at convergence with respect to n and N_t .

We treat N_s in a somewhat different manner. The spatial representation within the box should be refined as order and/or number of steps increase but we are unaware of any study of LPT that did so. Here, we will study one example with smooth initial conditions to establish that for sufficiently large grids the dominant error is set by Lagrangian order and is insensitive

Table 1. Table of parameters for the numeric tests presented in §3. Here, n is Lagrangian order, N_t is number of geometrically spaced steps, N_s is spatial grid size, Δt is the total time, t_0 is the initial time. The rms sub-scripted quantities are root mean square of δ , the initial density contrast, \mathbf{F}_δ , the initial first order acceleration, and $\mathbf{v}^{(L/T)}$, the initial velocity (longitudinal, transverse). Each test is discussed in the Section noted. 1D means a one dimensional density and velocity profile. ‘Top-hat’ means a compensated top-hat smoothed by a fixed Gaussian and including a non-radial, smooth velocity perturbation. ‘Exact’ refers to the analytic solution given for special initial conditions (Model I in Buchert et al. 1997).

Section	Type	n	N_t	N_s	$\frac{\Delta t}{t_0}$	δ_{rms}	\mathbf{F}_{rms}^δ	\mathbf{v}_{rms}^L	\mathbf{v}_{rms}^T
3.3	1D	1	1-4	16	0.75	0.007	0.112	0.007	0
3.4	Exact	3	1	16	.5	1.22	0.11	0.11	0
3.5	Top-hat	2	1	24-64	0.75	0.72	0.05	0.03	0.042
3.6.1	Zel’dovich	1-3	1-5	16	0.75	0.077	0.687	0.687	0
3.6.2	Generic	1-3	1-6	16	0.75	0.077	0.687	0.270	0.523

to grid size. For the remaining applications we argue (on a case by case basis) that grid-related errors are so small that convergence can be studied while holding N_s large and fixed.

This strategy is a reasonable but not rigorous approach to testing a method’s convergence in a comoving, periodic volume. It is also important to note that making the comoving box larger may be crucially important for achieving accurate physical results. This is distinct from solving a given problem in a given box. For example, if the box holds a finite subset of a larger physical system (e.g. the universe) and one is interested in mean quantities of the larger system then one might need to consider ever bigger boxes. Or, if the physical system in the box obeys different boundary conditions (e.g. isolated not periodic) then one might need to increase the physical size. In these situations convergence to the physical answer of interest will require that the grid density N_s/L and box size L increase without bounds.

3.2 Initial conditions

At the initial time t_0 , the system is completely specified by the choice of cosmology, the initial density field $\delta_{OBS}(\mathbf{Y}, t_0)$ and the peculiar velocity $\mathbf{v}_{OBS}(\mathbf{Y}, t_0)$. Table 1 gives a list of various parameters for the test runs presented here.

(i) All tests are done in an $\Omega = 1$ Einstein-deSitter cosmology over time intervals short enough that perturbations do not collapse to form multi-stream flows.

(ii) The initial conditions satisfy $\mathbf{v}_{c,0} = 0$. This choice of convenience allows us to characterize the peculiar velocity initial conditions completely and directly in terms of transverse and longitudinal content. It has no essential impact on the general conclusions derived from the testing.

(iii) The tests cover both special and generic initial conditions. Special initial conditions possess non-trivial symmetries. For example, it is well-known that transverse modes decay with time in expanding cosmologies. Practical cosmological simulations typically begin by setting $\mathbf{v}_{EB}^T(\mathbf{X}, t_0) = 0$; such initial conditions are special by this criterion. We also consider generic initial conditions to exercise the full dynamics.

3.3 Evolution of 1D perturbations

First order LPT is well-known to be an exact method for treating one dimensional problems prior to particle crossing (Peacock 1999). An ‘exact’ solution is directly found by quadrature irrespective of the identification of the EB frame. Here we compare exact results of this sort to answers generated by our general 3D numerical implementation of LPT re-expansion.

This comparison serves as a minimal check on the full code at first Lagrangian order because it involves all the basic elements of the most general calculation: the Fourier representation of spatial functions, solution of the ordinary differential equations for the time-dependent coefficients in the LPT expansion, evaluation of frame shifts and the interpolation from one Lagrangian grid to another. The solution of this simple problem exercises the entire re-expansion LPT methodology. No special modifications were made to the 3D code for carrying out this test.

The initial density and velocity perturbations were taken to be one dimensional functions consisting of a single Fourier component $\delta(\mathbf{X}, t_0) = 0.01 \cos 2\pi X_1/L$ and $\mathbf{v}(\mathbf{X}, t_0) = 0.01\{\cos 2\pi X_1/L, 0, 0\}$, where L is the comoving length of the box and X_1 is the component along the x -axis. With this choice the initial velocity and acceleration are *not* proportional and we expect non-zero frame shift terms. Calculations were made at Lagrangian orders $n = 1 - 3$, for $N_t = 1 - 4$ steps covering a

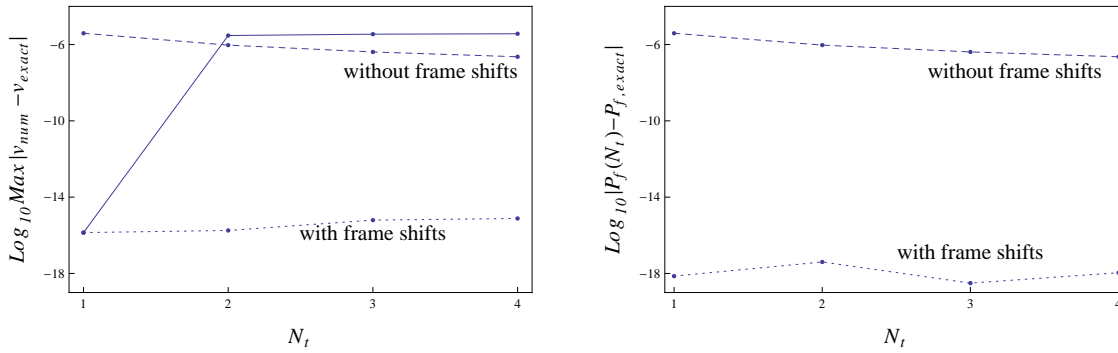


Figure 2. Left hand panel: the dotted line shows the maximum difference of numerical and quadrature-derived, exact answers when frame shifts are included in the numerical answer; the dashed line shows the same information when frame shifts are omitted from the numerical answer. Only when shifts are included do the numerical answers agree with the exact ones to machine precision. The solid line shows differences in single and multi-step numerical answers in the absence of frame shifts (none of these are “exact”). Right hand panel: test of momentum conservation for the numerical runs with (dotted) and without (dashed) frame shifts.

fixed total time Δt with time steps $t_i = t_0(1 + \Delta t/t_0)^{i/N_t}$ for $0 \leq i \leq N_t$. Regridding was done by solving equation (73) after each step.

Exact and numerical results are compared in the observer’s frame at the final time. As expected, the contributions to the solution at second and third order were zero to machine precision. The left panel of figure 2 shows the errors (maximum absolute velocity difference on the grid between exact and numerical results) as a function of the numbers of steps taken to reach the final time. The lower dotted line at roughly the round off level of computation (marked “with frame shifts”) shows that essentially perfect agreement with the exact answer is achieved for both single and multiple steps. This result validates (at first order) the implementation of LPT re-expansion. Note that a sequence of exact first order calculations is exact.

Frame shifts play an essential part in the numerical calculation. We repeated the calculation except that we imposed $\Delta \mathbf{x} = \Delta \dot{\mathbf{x}} = 0$ in equation (60) and equation (61). This omits the frame shifts. In left panel of figure 2 the upper dashed line shows the results obtained. There is an easily detected error with respect to the exact answer, an error present even for single step LPT.

Another useful comparison may be made between numerical single and multi-step calculations even if one is ignorant of the “exact” solutions. As we have already shown above when frame shifts are included single and multi-step first order LPT calculations are equivalent. However, if one omits the frame shifts this equivalency is broken. The solid line shows the difference between the numerical results for runs of a single step and those of multiple steps when all frame shifts are omitted. The explanation is simple: none of the answers is exactly right and the discrepancies are tied to different numbers of missing frame shifts.

The right hand panel of figure 2 shows a test of momentum conservation for calculations with and without frame shifts and for varying numbers of steps. With frame shifts the numerical calculation achieves round off levels of accuracy; without them the deficiency in the conservation law is easily detected and, moreover, does not improve as the interval in time is refined.

Taken together these simple tests help validate the method and underline the crucial importance of including the frame shifts.

3.4 Exact solutions

An excellent check is Model I in Buchert et al. (1997). It is an exact analytic result for one step in the EB frame at the first three orders for special initial conditions. Our numerical results agree with the analytic results to machine precision for all three orders. The special symmetry of the initial data implies that many of the spatial functions of the full general scheme vanish. The first, second and third orders comprise 2, 3 and 16 non-zero terms, respectively, and correspond to 2/3, 1/3 and 1/4 of the total number of possible terms at each order. The agreement using the full set of possible terms confirms that the both the time and space pieces of non-zero terms are encoded correctly. The agreement provides a consistency check for the spatial terms that vanish but says nothing conclusive about the temporal parts of these particular terms.

This check is essentially independent of the question of frame shifts. The analytic expressions for the frame shifts are exactly zero at all three orders. The numerically derived frame shift gave the same result to machine precision. It is not clear if the frame shifts continue to be zero at all higher orders, but for the purposes of this test we are concerned only with the first three orders.

Ideally one would construct more general test cases to check all possible terms in the code. Unfortunately, the method

of constructing ‘local forms’ (B94) is cumbersome and involves guessing the correct solution for the Lagrangian displacement at each order so that the divergence and curl match the source terms order-by-order. We have utilized the checks against all the published solutions of which we are aware.

3.5 Top-hat with fixed smoothing

The idealized configuration for this test is an overdense sphere surrounded by a compensating region and an infinite homogeneous background. If the initial velocity perturbation is zero the solution is simple and analytic. There are two practical issues that potentially interfere with running tests starting from this sort of initial data. The computational volume is intrinsically periodic and the computational method is designed to handle continuous not discontinuous spatial distributions.

A periodic configuration necessarily includes interactions between neighbouring boxes because exact spherical symmetry is not maintained in an approximate numerical solution. A suitably compact configuration limits these errors and the difference between the isolated and periodic versions can be made negligibly small.³ In principle, the top-hat is an excellent problem for validating the LPT expansion since the (isolated) solutions for the displacement and density can be computed analytically *order by order*. Numerical results can be compared to analytic ones at a given order (NC11). The significant complication is that the exact top-hat profile is discontinuous along the boundaries between the overdense sphere, the vacuum compensating region and the outer region of average density. Such discontinuities induce Gibbs phenomenon in the spatial Fourier representation and mask differences between expected and observed solutions. In principle, one can make the grid sufficiently large to overcome this interference but we do not attempt to do so here because the convergence is very slow. That means we must rely on indirect checks that the higher order terms in the LPT expansion are correct.

Here, we smooth the top-hat density field by a Gaussian with fixed width σ and also impose a smooth velocity field. The resulting velocity profile has both longitudinal and transverse velocities. The details of the configuration can be found in Appendix F. The exact solution is unknown so we discuss convergence using Cauchy differences for quantity f

$$\mathcal{E}_f(\alpha; \alpha') \equiv \sqrt{\langle (f^{\alpha'} - f^\alpha)^2 \rangle_q}, \quad (74)$$

where α and α' label one or more of n , N_t or N_s (with the other parameters held fixed) and q is the coordinate system used. We take $f = \delta$ for density and v for velocity at the final time. For $f = v$ all three velocity components are included.

We calculate a single step of small size so that the final time is well before collapse. The assessment of convergence involves Cauchy differences formed with runs having different grid resolutions and Lagrangian orders, e.g. $\alpha = \{N_s, n\}$ and $\alpha' = \{N_s + 1, n + 1\}$. The spectral representation of spatial functions suggests that if grid errors dominate then the Cauchy differences will decrease exponentially with N_s . Conversely, if errors in the series expansion in LPT dominate then the scaling will be exponential with n . This implies a sharp transition from errors dominated by grid resolution to errors dominated by Lagrangian order.

Runs with $16 \leq N_s \leq 48$ and $1 \leq n \leq 3$ were carried out for fixed smoothing. We evaluated the Cauchy differences as the grid was refined ($\mathcal{E}(N_s; N_s + 8)$ at fixed n) and then as the Lagrangian order was increased ($\mathcal{E}(n; n + 1)$ at fixed N_s) for $q = Y$ (on the OBS Lagrangian grid). Figure 3 shows the results for the density. The Cauchy differences for varying grids are virtually identical for $n = 1 - 3$ (this is not obvious from the figure, because the lines for different n overlap). The Cauchy differences for varying Lagrangian do not depend upon N_s (this is obvious from the fact the Cauchy differences are basically horizontal lines). Define the grid crossover $N_s^*(n)$ to be the value of N_s that satisfies $\mathcal{E}(\{n, N_s\}; \{n, N_s + 8\}) = \mathcal{E}(\{n, N_s\}; \{n + 1, N_s\})$ for a given n . The behaviour of the formal measure of convergence is

$$\mathcal{E}(\{n, N_s\}; \{n + 1, N_s + 8\}) \sim \begin{cases} \mathcal{E}(\{n, N_s\}; \{n, N_s + 8\}) & \text{if } N_s < N_s^* \\ \mathcal{E}(\{n, N_s\}; \{n + 1, N_s\}) & \text{if } N_s > N_s^* \end{cases} \quad (75)$$

The grid-related refinement dominates in the first case and order-related refinement in the second. The figure makes clear that the spatial differences decline exponentially with N_s (as they should for a spectral method) and the analytic structure for the LPT expansion suggests that order errors decline exponentially with n (this will be tested more directly in a succeeding section). One surmises that for two sources of exponential errors, the transition N_s^* should be a linear function of n .

The specifics of the transition from grid to order-dominated convergence are problem dependent. We have investigated initial conditions which differ from those above only in the degree of smoothing used (choice of σ). We find N_s^* is larger when initial data is less smooth and vice-versa.

The practical upshot is that if the solution is smooth and $N_s > N_s^*$ then the spatial errors are much smaller than changes

³ The Fourier representation of the density guarantees that the mass within each box is exactly equal to the background value. The identical symmetries of the Cartesian grid within the box and of the arrangement of the surrounding periodic copies guarantee that the dipole interactions between copies vanish. Therefore, the leading interaction that distinguishes the isolated from the periodic problem is a quadrupole term. It is $\sim 10^{-0.162N_s/L^4}$ for the configuration studied. This is roughly equivalent to machine precision at $N_s = 100$ and is very small compared to the truncation errors studied here.

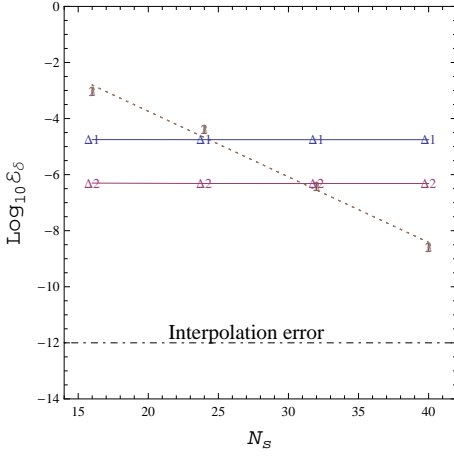


Figure 3. Convergence of the solution as the size of the spatial grid or the Lagrangian order is increased. Cauchy differences of density on the OBS Lagrangian grid are plotted. The dotted line traces the differences for calculations having increasing numbers of grid points (N_s and $N_s + 8$) at fixed Lagrangian orders ($n = 1, 2$ and 3). In fact, the calculated differences, labeled by n , all overlap. The straight dotted line indicates the exponential convergence expected for a spectral method. The solid, horizontal lines are Cauchy differences with respect to Lagrangian order (Δn refers to orders n and $n + 1$) at fixed N_s . Both types of errors are generally present. For small grids the grid-related spatial errors dominate and for large grids the Lagrangian-related finite order errors dominate. The crossover from N_s -dominated to n -dominated errors occurs at N_s^* . Additional calculations (not shown) demonstrate that N_s^* is smaller for smoother initial data. All the errors shown are much larger than the interpolation error shown by the dashed-dotted line.

associated with incrementing the Lagrangian order or decreasing the step size over finite ranges of n and N_t , respectively. We attempt to conduct all the rest of our tests in the limit $N_s > N_s^*$ when the grid errors are negligible.

3.6 Convergence with Lagrangian order n and number of steps N_t

This section presents tests of convergence with Lagrangian order n and number of steps N_t for initial conditions arising from a random Gaussian field at fixed spatial grid size. Two types of initial data are considered: Zel’dovich initial conditions (velocity proportional to the acceleration field; irrotational flow) and generic initial conditions (initial velocity chosen arbitrarily from random Gaussian fields; transverse and longitudinal components present and of comparable size). We focus on the truncation error for Lagrangian order n and re-expansion frequency N_t . We choose grids, initial conditions and time intervals for evolution for which we can be reasonably sure that grid-related errors at fixed N_s are so small that they do not interfere with the Cauchy differences for varying n and N_t .

We proceed as follows. The power in the initial data is limited to frequencies less than half the Nyquist frequency. In this discussion, we refer to wavenumbers as ‘frequency’ ($k = 2\pi/X$), not to be confused with the re-expansion frequency N_t . For box-length L and grid size N_s , the magnitude of the Nyquist frequency is $\pi N_s/L$. Since gravitational dynamics is intrinsically non-linear we know that the power in these initially zeroed modes will grow as collapse proceeds. Ultimately, any power that reaches or exceeds the Nyquist frequency will manifest as error since the Nyquist frequency is fixed because the grid is fixed. The size of the power in the vicinity of the Nyquist frequency is taken to be a surrogate for error incurred by using a finite grid. We monitor the power that builds up to make sure that the spatial errors remain negligible.

The power in the Nyquist frequencies is

$$P_{f,Nyq} = \sqrt{\frac{1}{N_s^3} \sum_{(\mathbf{k})} |\tilde{f}^{N_t}(\mathbf{k})|^2} \quad (76)$$

where (\mathbf{k}) is the set of wave numbers having a Cartesian component equal to the Nyquist frequency (or, we can monitor the power within a given range of the Nyquist value). Consider, for example, the Cauchy difference with respect to N_t on the OBS Lagrangian grid. This may be rewritten using Parseval’s theorem (Press et al. 2002)

$$\mathcal{E}_f(N_t; N_t') = \left(\frac{1}{N_s^3} \sum_{\mathbf{x}} |f^{N_t'}(\mathbf{x}) - f^{N_t}(\mathbf{x})|^2 \right)^{1/2} = \left(\frac{1}{N_s^3} \sum_{\mathbf{k}} |\tilde{f}^{N_t'}(\mathbf{k}) - \tilde{f}^{N_t}(\mathbf{k})|^2 \right)^{1/2}, \quad (77)$$

where \tilde{f} is the Fourier transform of f defined as $\tilde{f}_m = N_s^{-1/2} \sum_{l=1}^{N_s} f_l e^{2\pi i(m-1)(l-1)/N_s}$. The maximum contribution to the total that comes from the Nyquist modes is

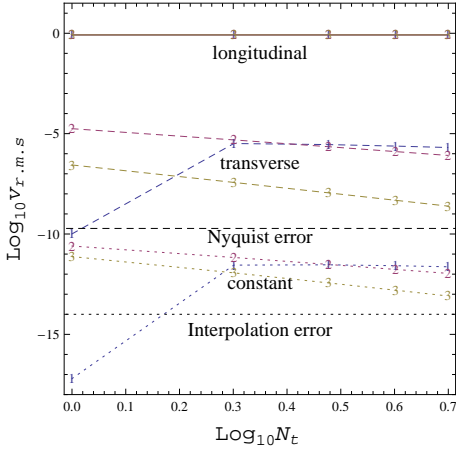


Figure 4. Root mean square of $\mathbf{v}^{(L)}$ and $\mathbf{v}^{(T)}$ and \mathbf{v}_c at the final time in the observer frame for the Zel’dovich initial conditions as a function of N_t the number of steps taken. Results for Lagrangian orders $n = 1 - 3$ have different colours and plot markers. Note that transverse components converge to zero in agreement with Kelvin’s theorem.

$$\sqrt{\frac{1}{N_s^3} \sum_{(\mathbf{k})} |\tilde{f}^{N_t'}(\mathbf{k}) - \tilde{f}^{N_t}(\mathbf{k})|^2} \lesssim 2 \sqrt{\frac{1}{N_s^3} \sum_{(\mathbf{k})} |\tilde{f}^{N_t}(\mathbf{k})|^2} = 2P_{f,Nyq}. \quad (78)$$

where the Nyquist components for N_t and N_t' are estimated to be of the same order of magnitude. When $\mathcal{E}_f(N_t; N_t') \gg P_{f,Nyq}$ we infer that the uncalculated finite grid errors are small compared to the calculated Cauchy differences. Likewise, when $\mathcal{E}_f(n; n') \gg P_{f,Nyq}$ we infer grid errors are small compared to the Cauchy differences for n . The fractional overdensity and peculiar velocity are not independent. We always use $\max_{f=\{\delta,v\}} P_{f,Nyq}$ in the figures that follow.

3.6.1 Zel’dovich initial conditions

The initial density is chosen to be a specific realization of a random Gaussian field and the initial peculiar velocity is set to be proportional to the acceleration at each point (Appendix D). The initial conditions satisfy $\mathbf{v}_c(t_0) = 0$. We calculated evolution over the same time interval for Lagrangian orders $n = 1 - 3$ and frequency of re-expansion $N_t = 1 - 5$.

Before presenting the convergence results let us first discuss an important feature of this flow. The velocity is irrotational at the initial time in the observer frame. Kelvin’s theorem states that for an ideal fluid under the influence of a conservative force, the velocity circulation around a closed contour comoving with the fluid stays constant in time. As a consequence, the vorticity of the velocity field is conserved. In particular, if the fluid is irrotational initially it stays irrotational (Landau & Lifschitz 1998; EB97).

Kelvin’s theorem applies to the exact dynamics in the Eulerian coordinate system. Although the initial conditions are irrotational in both Eulerian and Lagrangian systems, the Lagrangian calculations do not preserve irrotational flows in the Lagrangian coordinate system because there is no Lagrangian version of Kelvin’s theorem. If the Lagrangian calculation were exact then the flow would satisfy the exact conservation law for circulation after transformation back to the Eulerian coordinate system.

Our calculation is a finite order Lagrangian calculation with finite step size. We expect the exact Eulerian result that the flow should be irrotational (at any time) will emerge only as convergence is achieved. All non-zero transverse components in the OBS frame are errors and should necessarily diminish as the calculation is refined.

Figure 4 summarizes the scale of different velocity components at the final time in the OBS frame as a function of N_t for calculations at Lagrangian orders $n = 1 - 3$. In all cases the longitudinal component dominates and the transverse term is small by comparison. The transverse term decreases as N_t increases and as n increases. Both these trends show that solution behaves qualitatively in accord with Kelvin’s theorem.

Three other important scales are indicated on figure 4. The interpolation error is very small, consistent with the effect of machine precision; it is inconsequential for all our considerations. The Nyquist error provides an estimate of the error associated with the spatial grid. It is considerably larger than interpolation error but less than the scale of the transverse velocities mentioned above. Finally, the mean peculiar velocity \mathbf{v}_c (labeled “constant” because it does not depend upon position) is shown. As discussed in §2.8 \mathbf{v}_c is generally non-zero. In this run, the Zel’dovich initial conditions dictate $\mathbf{v}_{c,0} = 0$ and the time interval of evolution is small. Hence, the final \mathbf{v}_c is small in the sense of being no bigger than the Nyquist error. We infer that frame shifts play no essential role in these particular results.

Now consider the Cauchy differences for the solutions in figure 5. The upper panel presents the results for density,

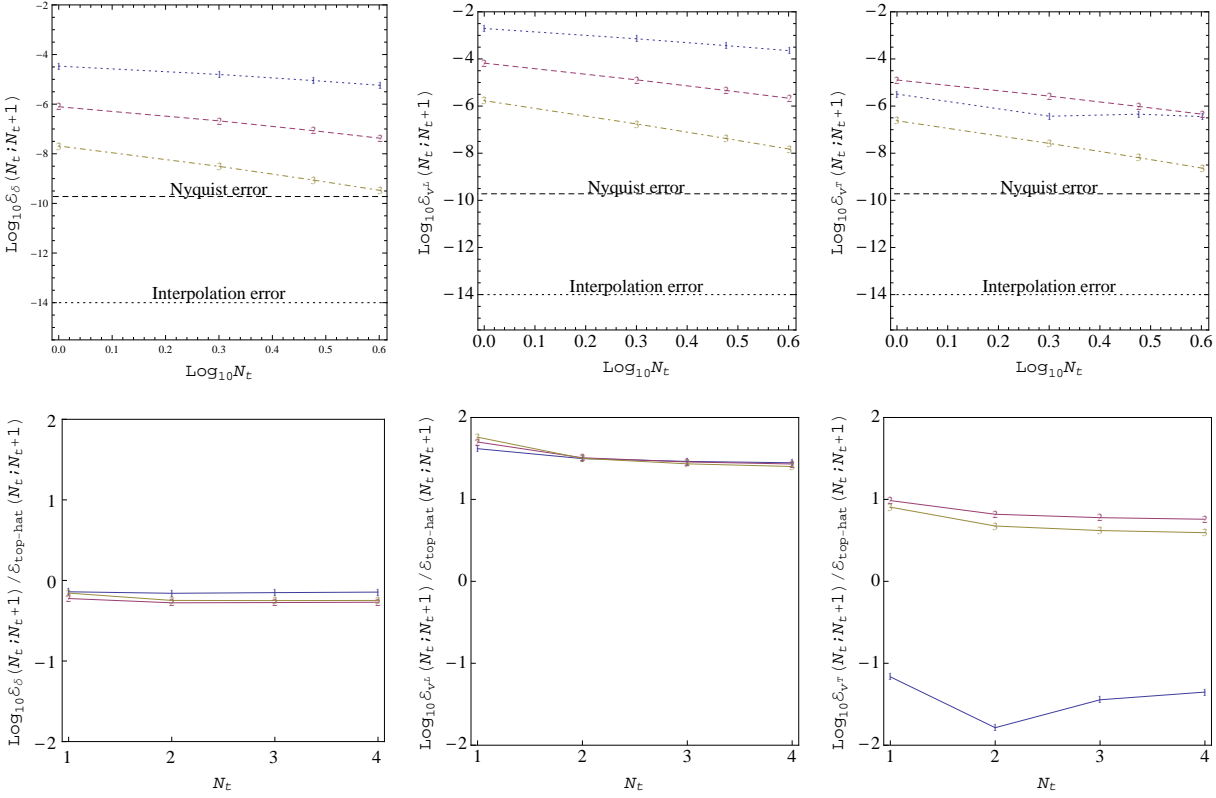


Figure 5. Convergence with respect to frequency of re-expansion for Zel'dovich initial conditions. Top panel: Cauchy differences at the final time \mathcal{E}_δ , \mathcal{E}_{vL} , \mathcal{E}_{vT} (comparing $N_t, N_t + 1$ for fractional overdensity, longitudinal peculiar velocity and transverse peculiar velocity, respectively). Nyquist error and interpolation error levels lie below those of the Cauchy differences and do not interfere. For all variables, at any order, the error decreases as the N_t increases. The rate of convergence is better for larger Lagrangian order n . Bottom panel: the ratio of Cauchy differences in the inhomogeneous calculation to those of the top-hat. It is noteworthy that the ratio is roughly constant for larger N_t and n . This provides a confirmation that the theoretical top-hat convergence rate describes the inhomogeneous case.

longitudinal and transverse components of velocity (left to right) in the OBS Eulerian frame as the number of steps N_t changes. Lines are labeled by Lagrangian order n . The Nyquist and interpolation errors lie below the Cauchy differences indicating that the truncation errors for order and frequency of re-expansion have been isolated from the effects of grid size and numerical precision. The slope of the lines slightly increases with higher n indicating faster convergence.

For the top-hat it was found theoretically, and confirmed empirically, that for a small time step $\Delta t/t_0 \ll 1$ the Cauchy differences decreased with N_t and n as

$$\mathcal{E}_{top-hat}(N_t; N_t + 1) \sim |g_{N_t+1, n} - g_{N_t, n}| \quad (79)$$

$$\mathcal{E}_{top-hat}(n; n + 1) \sim |g_{N_t, n}|, \quad (80)$$

where

$$g_{N_t, n} = K_{N_t, n} \cos \theta \sin^n \theta \Delta^{n+1} \left(\frac{\Delta t}{t_0}\right)^{n+2} \quad (81)$$

$$K_{N_t, n} = \frac{1}{9} \left(\frac{-2}{3}\right)^n \left(\frac{N_t - \frac{n}{2+n}}{N_t^{n+1}}\right). \quad (82)$$

The quantities Δ and θ characterize the strengths of the initial density and velocity perturbations ($\delta = \Delta \cos \theta$ and $\delta_v = \Delta \sin \theta$). Note that $g_{N_t, n}$ scales exponentially with Lagrangian order n for any given N_t . This is expected because the n -th term in the LPT series is $\propto \epsilon^n$, where ϵ is the magnitude of the initial perturbation. Conversely, the theoretical error scales as a power of the number of steps $\propto N_t^{-n}$ as N_t increases. The latter also implies that the slope steepens with Lagrangian order n .

The lower panel of figure 5 presents a quantitative comparison of the top-hat convergence rates to the more general problem that has been calculated. The figure shows the ratio of \mathcal{E} to that deduced previously for the top-hat. (For Zel'dovich initial conditions $\theta = \arctan(-1/3)$ and $\Delta = \sqrt{10}\delta/3$; we used the root mean square value for δ). The ratio is approximately constant implying that the convergence rates with respect to n and N_t for inhomogeneous initial conditions are close to those of the top-hat. The agreement is very good for the density and longitudinal velocity. The only anomaly appears to be related

to the relative size of the first and second order transverse velocity differences (far right panel). The second and third order terms scale as predicted theoretically.

The explanation is enlightening. One might first imagine that the cause was related to the fact that the top-hat collapse does not include any components of transverse velocity. Then it would be unsurprising if the theoretical result failed to capture the apparent inversion in transverse components. But that is not what we find. The key point is already present in figure 4 which shows that the magnitude of the transverse velocity is very small after a single, first order step but much larger after a single, second order step or after multiple steps of first order.

We find the explanation is related to the way in which the Lagrangian system “recovers” the result implied by Kelvin’s theorem, i.e. that the transverse component in the Eulerian system should ultimately vanish. When the initial conditions satisfy velocity proportional to acceleration, the lowest order, non-vanishing contribution to the Lagrangian frame transverse velocity is third order (BE93; B94). However, the transformation from Lagrangian to Eulerian coordinates is essential, i.e. the transformation itself can contribute to the Eulerian transverse velocity. The Eulerian transverse velocity (defined as $\mathbf{w}_E(\mathbf{r}, t) = \nabla_r \times \mathbf{v}_{OBS}$) is equal to the Lagrangian transverse velocity (defined as $\mathbf{w}_L(\mathbf{Y}, t) = \nabla_Y \times \mathbf{v}_{OBS}$) plus ‘extra’ terms that are quadratic and cubic combinations of the displacement vector and its time derivative (see Appendix G)

$$\mathbf{w}_E(\mathbf{Y}, t) = \mathbf{w}_L(\mathbf{Y}, t) + \text{Terms}[\mathbf{p}, \dot{\mathbf{p}}] + \text{Terms}[\mathbf{p}, \mathbf{p}, \dot{\mathbf{p}}]. \quad (83)$$

When the calculation is done with a first order, single step LPT scheme for Zel’dovich initial conditions, these ‘extra’ terms vanish exactly and we get both $\mathbf{w}_L(\mathbf{Y}, t) = 0$ and $\mathbf{w}_E(\mathbf{Y}, t) = 0$ at all times. When the calculation is done with a second order, single step LPT scheme for Zel’dovich initial conditions, $\mathbf{w}_L(\mathbf{Y}, t) = 0$ at all times, but the ‘extra’ non-zero terms are third and higher order in the expansion parameter (‘extra’ terms that are second order vanish).

$$\mathbf{w}_E(\mathbf{Y}, t) = \mathbf{w}_L(\mathbf{Y}, t) + \mathcal{O}(\epsilon^3) \quad (84)$$

$\mathbf{w}_E(\mathbf{Y}, t) \neq 0$ except for the initial time. So, we have the unexpected consequence that a single step of a first order LPT calculation will yield zero Eulerian transverse velocity in the OBS frame but that a single step of a higher order calculation will generally yield a non-zero Eulerian transverse velocity. Both the first order and the infinite order calculations will satisfy Kelvin’s theorem. Of course, the first order solution is not exact and we can expect convergence only as the order increases. In general, with a n -th order calculation, one expects $\mathbf{w}_E(\mathbf{r}, t) = \mathcal{O}(\epsilon^{n+1})$ which relies on complicated cancellations between all terms of order less than n between the three pieces on the r.h.s. of equation (83).

Figure 4 shows that multiple steps of a first order scheme builds up a non-zero transverse velocity. This might appear to be at odds with the discussion above in which a single, first order step exactly satisfies Kelvin’s theorem. The reason is that even one step will generate a state where the initial proportionality between velocity and acceleration is broken. In subsequent steps even a first order LPT scheme can then give non-vanishing contribution to transverse velocity in the Eulerian frame (due to the second and higher order terms in the transformation between Eulerian and Lagrangian coordinates). Multi-step, first order calculations may generate transverse velocity. Convergence and consistency with Kelvin’s theorem is expected as the number of steps increase.

Ultimately, only the asymptotics matter: we have shown that refinements in order and/or step size both lead to smaller transverse motions in the Eulerian frame. Higher order Lagrangian schemes converge more quickly in the asymptotic limit. For example, in the top right hand panel the line for $n = 3$ lies below that for $n = 2$ and its downward slope (as a function of N_t) is greater.

We conclude that the LPT re-expansion converges for Zel’dovich initial conditions and, moreover, that it does so at a rate which is essentially identical to that theoretically derived in the case of the top-hat.

3.6.2 Generic initial conditions

In this test the initial density and peculiar velocity are independent realizations of a Gaussian random field. The latter has longitudinal and transverse components of comparable magnitude. We follow the evolution of the initial conditions for varying Lagrangian order ($n = 1 - 3$) and re-expansion frequency ($N_t = 1 - 6$). Figure 6 summarizes (left panel) the root mean square velocity at the final time and (right panel) the evolution of the transverse velocity. For the small time step considered here the longitudinal and transverse parts are still comparable at the final time but (right panel) the transverse mode decays $\propto 1/a$. Here, \mathbf{v}_c is greater than in the Zel’dovich case and points to the importance of frame shifts.

Figure 7 shows the Cauchy differences for changes in N_t . The differences decrease with increase in N_t and Lagrangian order n . The transverse term here behaves in a qualitatively identical manner to the longitudinal case (there is no low-order anomaly like that seen in the Zel’dovich case). The scaling of these errors closely follows the trend established for the top-hat (the graphs are not repeated here).

Our main conclusion drawn from the results for the generic test case is that the full gravitational dynamics has been successfully implemented in the LPT re-expansion method.

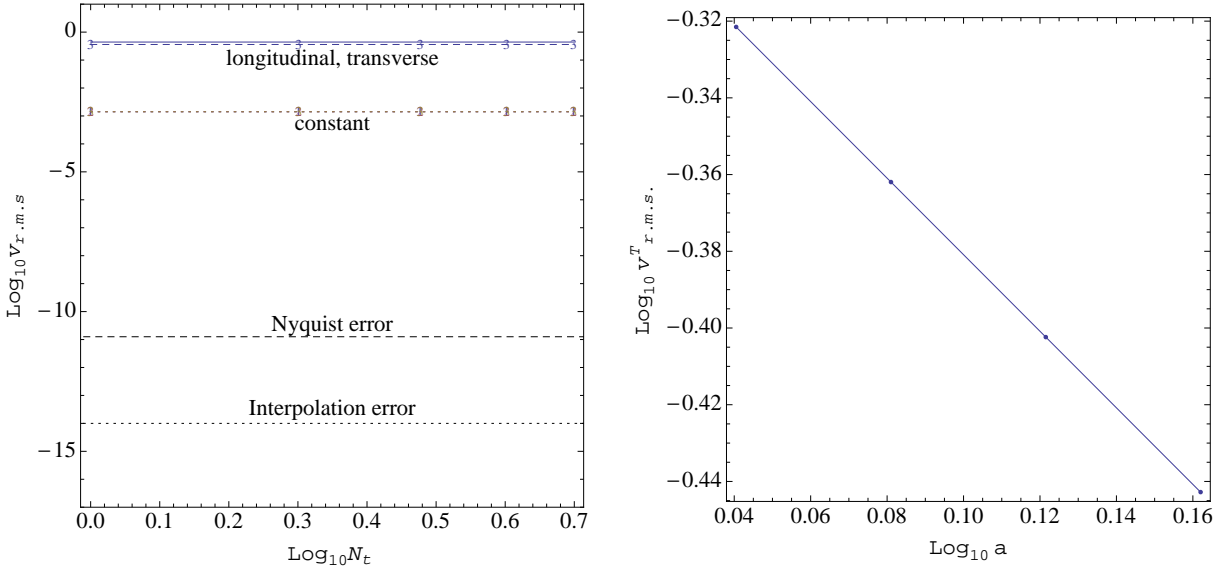


Figure 6. Root mean square of various components of the final velocity in the observer frame (left) and the transverse velocity as a function of the scale factor (right). The longitudinal and transverse components are roughly the same magnitude initially and, on account of the small time advanced, finally. However, on an expanded scale magnitude of the transverse velocity decreases $\propto 1/a$. Dots are data, line is the fit. The theoretically expected slope is -1 and best fit line has slope -0.99 . All orders have similar behaviour; first order data is shown here.

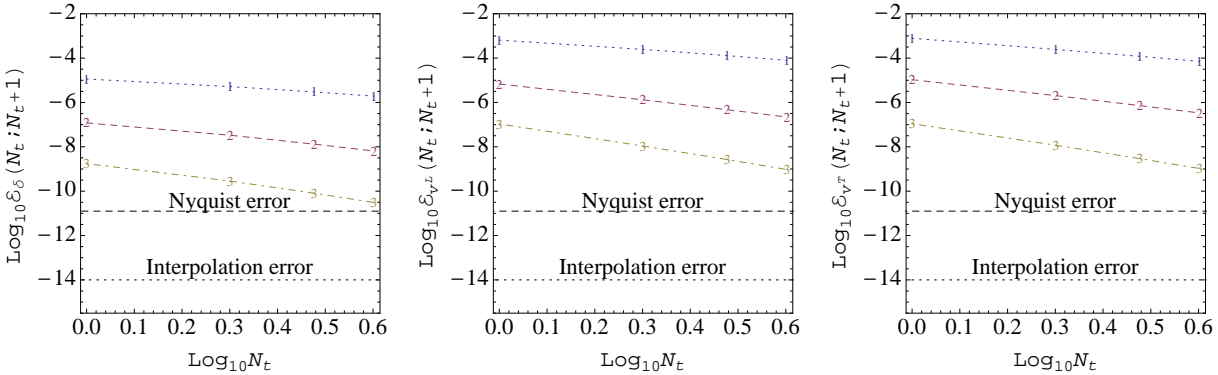


Figure 7. General initial conditions: convergence with respect to Lagrangian order and frequency of re-expansions. The coding of the graph is the same as figure 5. Cauchy differences for N_t decrease as N_t increases; the rate of convergence improves for higher Lagrangian order n . The scaling of these errors with respect to a top-hat is similar to the lower panel of figure 5 and is not shown separately here.

3.6.3 Frame shifts again

We had previously illustrated frame shifts in the simplest possible case, one-dimensional problems. Here we revisit the issue in the context of the general case just discussed. We will show that the numerical convergence as measured by the Cauchy differences is destroyed and momentum conservation broken when frame shifts are omitted.

Figure 8 compares convergence of the density field in calculations with (left) and without (right) frame shifts. The left panel shows the same sort of scaling with n and N_t as seen in the two previous sections. Increasing the Lagrangian order and/or increasing the frequency of re-expansion reduces the differences. The right panel shows an anomaly, that the Cauchy differences for $n = 2$ and $n = 3$ lie on top of each other. This implies that convergence with Lagrangian order is broken.

The lower panel compares momentum conservation error with (left) and without (right) frame shifts. The momentum, as defined in equation (65), is calculated at initial and final times, $\mathbf{P}(t_0)$ and \mathbf{P}_f , respectively. The former is known exactly from the choice of initial conditions. After the evolution \mathbf{P}_f is known numerically and it may be compared to the exact result $\mathbf{P}_{f, exact} = a(t_0)\mathbf{P}(t_0)/a_f$. We calculated the error as the absolute difference between the exact and approximate value summed in quadrature over the three directions. The figure (left) shows that conservation is achieved asymptotically with frame shifts.

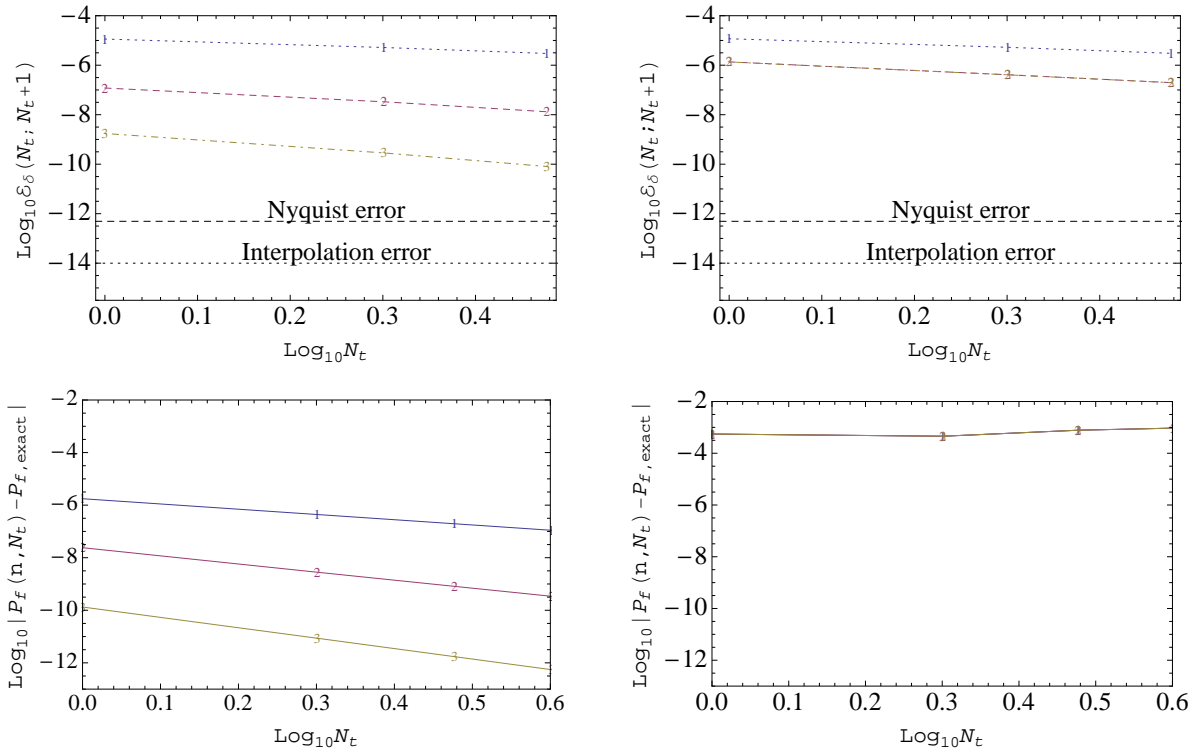


Figure 8. Frame shifts and momentum conservation (general case). Top panel: Cauchy differences for density with (left) and without (right) frame shifts. Bottom panel: momentum conservation errors with (left) and without (right) frame shifts. Frame shifts are crucial to ensure convergence with Lagrangian order and ignoring them leads to a breakdown of momentum conservation.

By contrast, there is no evidence for improvement when the frame shifts are omitted (right). Increasing the Lagrangian order and/or increasing the frequency of re-expansion reduces the error.

3.7 Summary of convergence tests

The tests indicate that the LPT re-expansion method works in principle and in practice for inhomogeneous initial conditions. This is the natural extension and generalization of our previous work on the top-hat model. These tests probe convergence when various combinations of grid size, Lagrangian order and/or re-expansion frequency are increased. Testing the rates separately has yielded results consistent with the underlying solution methodology (exponential in number of grid points for the spectral representation of spatial functions, exponential in Lagrangian order for the perturbation expansion, geometric in step size at fixed Lagrangian order). An essential part of the method is frame shifts. Ignoring them leads to violations of momentum conservation and breaks the theoretically expected convergence rates.

4 CONCLUSION

We have developed a new method to calculate the growth of large scale structure based on Lagrangian perturbation theory. It is designed to handle generic inhomogeneous perturbations on sub-horizon scales having non-relativistic velocities and weak gravitational fields. It can follow the system evolution until the formation of the first caustic.

Many of the fundamental ideas were first discussed in the context of spherical top-hat cosmologies in NC11. There we demonstrated the existence of limitations on the convergence of the series expansion which is the basis of LPT. We showed that even if one could work to infinite order in the LPT expansion parameter there are bounds in time that limit how far forward a single step can extend. Such limitations are more restrictive than the onset of particle crossings. To circumvent the bounds we introduced the idea of re-expanding the solution in overlapping time domains (“LPT re-expansion”). Our work generalized LPT from a single-step to a multi-step scheme permitting evolution all the way up to the onset of multi-streamed flow.

This paper extends the analysis from spherical top-hat cosmologies to generic initial conditions in the context of Newtonian cosmology. A new and important theoretical point is the existence of frame shifts. Frame shifts originate because the starting point of traditional derivations of the LPT series involves taking derivatives of the geodesic equation or its equivalent. The

perturbative theory and solution obtained in this way is insensitive to time-dependent translations and will generally not satisfy the original equations of motion unless this freedom is fixed (no such freedom was present in the spherical cases studied in NC11). We introduce two conceptual frames to explore the situation. The OBS frame is the frame in which the physical initial conditions are specified and the answer sought. The EB frame is the frame in which the perturbative solution is obtained via the formal LPT expansion described in EB97. We describe in detail how to transform from one frame to the other. The relationship between OBS and EB frames is non-trivial. For example, it is not set by a physically conserved quantity. In many instances frame shifts are required, e.g. in a finite cosmology simulation, the EB frame will generically differ from that of the preferred OBS frame tied to the cosmic microwave background. At each step one must determine the relationship anew. We argued that ignoring the frame shifts generically leads to a breakdown in momentum conservation.

The multi-step algorithm we have developed can be summarized as follows. Start with initial density and velocity defined in the OBS frame with Lagrangian coordinates equal to uniform Eulerian grid coordinates at time t . Transform quantities to the EB frame (the density remains the same, velocity differs by a constant). Use the EB formalism to advance the density and velocity in the EB frame from t to time $t + \delta t$ subject to the restriction imposed by the time of validity, the span over which the LPT expansion converges. Compute the frame shifts accumulated during the evolution and transform the EB solution back to the OBS frame at the end of the step. Interpolate the final OBS quantities onto the uniform Eulerian grid at time $t + \delta t$. These quantities serve as the initial data with new initial Lagrangian coordinates equal to Eulerian coordinate for the next step.

The algorithm was numerically implemented and tested. All tests were done in a $\Omega_m = 1$ cosmology over time intervals that obeyed the predicted time of validity. Since these are meant to be ‘proof of principle’ tests we performed them on grids of small size.

Some tests involve comparisons to exact answers. The solution for a simple, plane-parallel problem can be written down without reference to LPT. Since first order LPT should produce an exact result this enables several different checks to be carried out. We showed that our first order LPT treatment with frame shifts matches the exact solution. We also established that ignoring the frame shifts gives rise to problems and inconsistencies. Several different lines of argument (involving momentum conservation, convergence, single versus multiple steps) substantiated the fundamental role of the frame shift even in the context of this simplest-of-all problems. Discrepancies introduced by ignoring frame shifts might go undetected for some specific initial conditions or in a single step scheme but they become clearly apparent even in this simple geometry for general initial data and/or while utilizing a multi-step scheme.

As a second exact comparison we tested our results against the analytic example given in Buchert et al. (1997). This allows a check of the implementation of the higher order LPT terms. This provided a complete check of the non-zero (spatial and temporal) terms up to third order and a consistency check that the spatial parts of all the other terms vanish. The specific numbers of each type of term are given in the text. The frame shift, which vanishes for this particular example, is also checked by this test.

Other tests involve situations where the exact answer is unknown and we focus on whether the convergence of the algorithm agreed with theoretical expectations. There are three control parameters: grid size N_s , Lagrangian order n and the frequency of re-expansion N_t . We first discuss theoretical convergence to the exact answer. Generally, N_s and one (or both) of n and N_t must increase simultaneously. The refinement must be made subject to the time of validity criterion.

For diagnostic purposes we show it is possible to choose initial conditions and parameters such that errors are largely set by a single parameter. This allows us to study the nature of the convergence of that part of the calculation. To demonstrate convergence with grid size we represented the initial density and velocity with a spherical top-hat profile filtered with a Gaussian. We showed that for these smooth initial conditions, the errors due to the finite grid size decreased exponentially with N_s , when other errors due to Lagrangian order were negligible. This was in accordance with the expected behaviour because spectral methods are used to solve the spatial equations. Likewise, when the grid size errors are very small the convergence with Lagrangian order is exponential in accordance with the basic understanding that LPT is a power series expansion in the perturbation parameter. We show that there is a sharp transition from convergence being controlled by grid size N_s to it being controlled by Lagrangian order n .

For the remaining studies, we set N_s large enough that we could focus on the convergence with Lagrangian order n and/or the number of time steps N_t . We considered initial data based on a random Gaussian field. Two types of initial conditions were considered: Zel’dovich initial conditions, where the velocity was proportional to the acceleration field, and generic initial conditions, where the initial velocity includes both longitudinal and transverse components. Though unanticipated we discovered that the rate of convergence of these complicated examples scaled nearly identically as the rate of convergence for the simple top-hat cosmologies (whose rates were analytically derived and numerically confirmed in NC11). To summarize, the convergence with n is exponential and that with N_t is algebraic. The internal consistency for solutions achieved when varying n and N_t (a common asymptotic solution and Cauchy differences which diminish at the theoretically anticipated rate) provides strong evidence that the system is being solved correctly. We also demonstrated that when the frame shifts are omitted the convergence tests fail and conservation of momentum is violated.

We explored how Kelvin’s theorem is satisfied for situations in which the initial Eulerian vorticity vanishes. Kelvin’s

theorem implies that the Eulerian vorticity vanishes at all future times prior to the formation of caustics. Since this is an exact result it serves as a useful check on the end-to-end solution, i.e. the transformations between OBS and EB frames and the LPT calculation within the EB frame. We confirmed numerically that the magnitude of the Eulerian vorticity converges to zero in the asymptotic limit just as it should. This is a non-trivial check as can be seen from the following considerations. If the initial vorticity vanishes then vorticity as measured in the Lagrangian frame is generated at third and higher orders (for single step Lagrangian solution; BE93 and B94). What happens to these contributions in the OBS frame? They should vanish as the calculation order increases. The key is that vorticity as measured in the Lagrangian frame is not the same as vorticity as measured in the Eulerian frame. This can be seen in several ways. For example, a second order LPT calculation for the initial conditions described above yields zero vorticity in the Lagrangian frame (to second order) but this still gives rise to a non-zero vorticity in the Eulerian frame because of the transformation between the two frames. Alternatively, in a multi-step scheme, Eulerian vorticity is generated even with a first order LPT scheme. The appearance of Eulerian vorticity at a given finite order does not violate the Kelvin circulation theorem as long as the order of that contribution increases with the order of the calculation itself. This is the situation that is indicated by the numerical results. (Likewise, increasing the number of steps causes the magnitude of the Eulerian vorticity to diminish.) Prior studies have examined the density and/or the Lagrangian displacement and, to the best of our knowledge, these aspects of the solution have never been tested. The frame transformation is needed to achieve this consistency.

We now consider the future utility of this new method.

The choice of the exact number of time steps, Lagrangian order and grid size which govern the numerical errors will ultimately depend on the application at hand. The numerical errors can be made as small as desired. However, we have not addressed the important drawback of LPT, which is its inability to model physics beyond shell crossing. Real cosmological applications will be limited by the occurrence of multi-streaming. Any approximation to account for the velocity dispersion (Adler & Buchert 1999; Buchert, Domínguez, & Pérez-Mercader 1999; Morita & Tatekawa 2001; Tatekawa 2005) or alterations to the basic dynamics (such as the adhesion approximation; see reviews Sahni & Coles 1995; Gurbatov, Saichev, & Shandarin 2012) will introduce physical errors as opposed to the numerical errors with which we have dealt. The algorithm presented in this paper will require additional development to deal directly with shell crossing for most cosmological applications. Alternatively, a good physical understanding of the nature of the errors introduced by various approximations may suffice.

In general terms there are three main advantages of the LPT re-expansion method presented in this paper. (1) The smooth treatment of the density and velocity fields frees the results from particle-related shot-noise contamination (see Joyce, Marcos, & Baertschiger 2009 for a detailed discussion of this issue in the context of numerical simulations). (2) The method can be fine-tuned to control the numerical error by changing the number of time steps and/or the Lagrangian order. (3) The scheme is designed to deal with general initial conditions including cases where the velocity fields may have a rotational component. Although this generality has always been implicit in LPT's formal development (Moutarde et al. 1991; B92), it has mostly been omitted in applications to real cosmological problems because vortical modes decay away in expanding cosmologies. Working in full generality should permit an LPT based scheme to handle arbitrary initial data which develops during the course of later phases of evolution. In addition, given the recent interest in using information from peculiar velocities to constrain cosmological parameters, it should prove useful to be able to handle these modes even in the quasi-linear regime.

We envision several applications of our method, particularly where accurate results are desired on quasi-linear scales. We mention a few of them below.

One important application is the Baryon Acoustic Oscillation (BAO) signal reconstruction. The detection of the BAO signal in the SDSS survey (Eisenstein et al. 2005) implies that measurements of this sort will provide a powerful means to constrain cosmological parameters. Flows on quasi-linear scales cause the observed signal to have lower amplitude and peaks slightly shifted with respect to linear theory predictions. As observational probes improve, a sub-percent level precision determination of the BAO scale will require very accurate reconstruction (Percival et al. 2010). Already techniques based on single step LPT have been proposed (e.g. Eisenstein et al. 2007; Matsubara 2008; Tassev & Zaldarriaga 2012). Our multi-step re-expansion algorithm can be used to achieve the needed level of error through control of a combination of time-step and Lagrangian order. Error control in perturbation techniques is of course an important element for the establishment of cosmological constraints (Carlson, White, & Padmanabhan 2009).

Another important application is modelling the peculiar velocity field and investigating the density-velocity relation. The peculiar velocity information is encoded in the observed redshift space distortions (RSD) seen in galaxy surveys. Recent measurements (e.g. Guzzo et al. 2008) have demonstrated that this information has the power to distinguish between various cosmological models. In linear theory, the density and velocity divergence are proportional and consequently, the ratio of the redshift space to real space power spectra is a constant. Numerical simulations show a breakdown of that prediction, starting at scales as large as $k \sim 0.03h^{-1}$ Mpc (Jennings, Baugh, & Pascoli 2011), which would normally be regarded as well within the linear regime. Understanding these scales is important. Analytical methods based on perturbation theory (for e.g., Bernardeau 1992; Kitaura et al. 2012) or based on spherical dynamics (Bilicki & Chodorowski 2008; Nadkarni-Ghosh 2013) give approximate answers but definitive answers will require a more simulation-based approach. LPT re-expansion will be ideal since it is intrinsically smoother than particle-based approaches. The current code can track all components of the

velocity field enabling detailed investigations of RSD power spectrum as has recently been discussed by Zhang, Pan, & Zheng (2012).

Other important applications include the evolution of non-Gaussianity and the estimation of the growth of voids. If and when shell crossing is accurately handled the method of LPT re-expansion may nicely complement existing methods for modeling the growth of large scale structure.

ACKNOWLEDGMENTS

A part of this work contributed to the Ph. D. thesis of SN at Cornell University. We thank Ira Wasserman and Rachel Bean for useful discussions. DFC acknowledges support of NSF Grant No. AST-0406635 and NASA Grant No. NNG-05GF79G. SN acknowledges the hospitality of the Astronomy department at Cornell University during subsequent visits. The authors thank Thomas Buchert for useful discussions and pointing out additional references.

REFERENCES

- Adler S., Buchert T., 1999, *Astronomy and Astrophysics*, 343, 317324
- Bernardeau F., 1992, *The Astrophysical Journal*, 390, L61
- Bilicki M., Chodorowski M. J., 2008, *Monthly Notices of the Royal Astronomical Society*, 391, 1796
- Bouchet F. R., Colombi S., Hivon E., Juszkiewicz R., 1995, *Astronomy and Astrophysics*, 296, 575
- Bouchet F. R., Juszkiewicz R., Colombi S., Pellat R., 1992, *Astrophysical Journal*, 394, L5L8
- Buchert T., 1989, *Astronomy and Astrophysics*, 223, 924
- Buchert T., 1992, *Monthly Notices of the Royal Astronomical Society*, 254, 729737
- Buchert T., 1994, *Monthly Notices of the Royal Astronomical Society*, 267, 811
- Buchert T., Domínguez A., Pérez-Mercader J., 1999, *Astronomy and Astrophysics*, 349, 343353
- Buchert T., Ehlers J., 1993, *Monthly Notices of the Royal Astronomical Society*, 264, 375387
- Buchert T., Götz G., 1987, *Journal of Mathematical Physics*, 28, 2714
- Buchert T., Karakatsanis G., Klaffl R., Schiller P., 1997, *Astronomy and Astrophysics*, 318, 110
- Buchert T., Melott A. L., Weiss A. G., 1994, *Astronomy and Astrophysics*, 288, 349
- Caldwell R. R., Dave R., Steinhardt P. J., 1997, astro-ph/9708069, *Phys.Rev.Lett.*80:1582-1585,1998
- Carlson J., White M., Padmanabhan N., 2009, *Physical Review D*, 80, 43531
- Catelan P., 1995, *Monthly Notices of the Royal Astronomical Society*, 276, 115
- Cooray A., Holz D. E., Caldwell R., 2010, *Journal of Cosmology and Astro-Particle Physics*, 11, 015
- Crocce M., Pueblas S., Scoccimarro R., 2006, *Monthly Notices of the Royal Astronomical Society*, 373, 369381
- Ehlers J., Buchert T., 1997, *General Relativity and Gravitation*, 29, 733764
- Eisenstein D. J., Seo H.-J., Sirko E., Spergel D. N., 2007, *Astrophysical Journal*, 664, 675679
- Eisenstein D. J. et al., 2005, *The Astrophysical Journal*, 633, 560
- Gurbatov S. N., Saichev A. I., Shandarin S. F., 2012, *Physics Uspekhi*, 55, 223
- Guzzo L. et al., 2008, *Nature*, 451, 541
- Jennings E., Baugh C. M., Pascoli S., 2011, *Monthly Notices of the Royal Astronomical Society*, 410, 2081
- Joyce M., Marcos B., Baertschiger T., 2009, *Monthly Notices of the Royal Astronomical Society*, 394, 751
- Karakatsanis G., Buchert T., Melott A. L., 1997, *Astronomy and Astrophysics*, 326, 873
- Kasai M., 1995, *Physical Review D*, 52, 5605, copyright (C) 2009 The American Physical Society; Please report any problems to prola@aps.org
- Kitaura F.-S., Angulo R. E., Hoffman Y., Gottlöber S., 2012, *Monthly Notices of the Royal Astronomical Society*, 425, 2422
- Landau L., Lifschitz E., 1998, *Fluid Mechanics*, Revised 2nd Edition. Butterworth-Heinemann
- Matarrese S., Pantano O., Saez D., 1993, *Physical Review D*, 47, 13111323
- Matarrese S., Pantano O., Saez D., 1994, *Monthly Notices of the Royal Astronomical Society*, 271, 513
- Matarrese S., Terranova D., 1996, *Monthly Notices of the Royal Astronomical Society*, 283, 400418
- Matsubara T., 2008, *Physical Review D*, 77, 63530
- Melott A. L., Buchert T., Weiss A. G., 1995, *Astronomy and Astrophysics*, 294, 345
- Monaco P., 1997, *Monthly Notices of the Royal Astronomical Society*, 287, 753770
- Monaco P., Theuns T., Taffoni G., 2002, *Monthly Notices of the Royal Astronomical Society*, 331, 587608
- Morita M., Tatekawa T., 2001, *Monthly Notices of the Royal Astronomical Society*, 328, 815
- Mota D. F., Shaw D. J., Silk J., 2008, *The Astrophysical Journal*, 675, 2948
- Moutarde F., Alimi J.-M., Bouchet F. R., Pellat R., Ramani A., 1991, *Astrophysical Journal*, 382, 377381
- Munshi D., Sahni V., Starobinsky A. A., 1994, *The Astrophysical Journal*, 436, 517
- Nadkarni-Ghosh S., 2013, *Monthly Notices of the Royal Astronomical Society*, 428, 1166
- Nadkarni-Ghosh S., Chernoff D. F., 2011, *Monthly Notices of the Royal Astronomical Society*, 410, 1454
- Novikov E. A., 1969, *Soviet Journal of Experimental and Theoretical Physics*, 30, 512
- Peacock J., 1999, *Cosmological physics*. Cambridge University Press
- Percival W. J. et al., 2010, *Monthly Notices of the Royal Astronomical Society*, 401, 2148
- Press W., Teukolsky S., Vetterling W., Flannery B., 2002, *Numerical Recipes in C++*. Cambridge University Press
- Rampf C., 2012, *Journal of Cosmology and Astro-Particle Physics*, 12, 004
- Rampf C., Buchert T., 2012, *Journal of Cosmology and Astro-Particle Physics*, 06, 021
- Rampf C., Rigopoulos G., 2012, *ArXiv e-prints*, 1210, 5446
- Rampf C., Wong Y. Y. Y., 2012, *Journal of Cosmology and Astro-Particle Physics*, 06, 018
- Sahni V., Coles P., 1995, astro-ph/9505005, *Phys.Rept.*262:1-135,1995
- Sahni V., Shandarin S., 1996, *Monthly Notices of the Royal Astronomical Society*, 282, 641645
- Scoccimarro R., 1998, *Monthly Notices of the Royal Astronomical Society*, 299, 10971118
- Scoccimarro R., Sheth R. K., 2002, *Monthly Notices of the Royal Astronomical Society*, 329, 629640

- Tassev S., Zaldarriaga M., 2012, *Journal of Cosmology and Astro-Particle Physics*, 10, 006
 Tatekawa T., 2005, *Physical Review D*, 71, 44024
 Tatekawa T., 2012, *ArXiv e-prints*, 1210, 8306
 Zel'dovich Y. B., 1970, *Astronomy and Astrophysics*, 5, 84
 Zhang P., Pan J., Zheng Y., 2012, *ArXiv e-prints*, 1207, 2722

APPENDIX A: MATHEMATICAL TRANSFORMATIONS

The section below outlines the transformations that are performed on equations (12) and (13) to change the dependent variable from $\mathbf{r} = \mathbf{r}_{EB}$ to \mathbf{X} . For simplicity we drop the subscript ‘EB’. The l.h.s. of equation (12) is

$$\nabla_{\mathbf{r}} \cdot \ddot{\mathbf{r}} = \frac{\partial \ddot{r}_i}{\partial r_i} = \frac{\partial \ddot{r}_i}{\partial X_l} \frac{\partial X_l}{\partial r_i}. \quad (\text{A1})$$

Einstein’s repeated summation convention is followed throughout. The inverse transformation from X -space to r -space is given as

$$\frac{\partial X_l}{\partial r_i} = \frac{1}{2J} \epsilon_{lmn} \epsilon_{ijk} \frac{\partial r_j}{\partial X_m} \frac{\partial r_k}{\partial X_n}, \quad (\text{A2})$$

where

$$J = \text{Det} \left(\frac{\partial r_i}{\partial X_j} \right) = \epsilon_{abc} \frac{\partial r_1}{\partial X_a} \frac{\partial r_2}{\partial X_b} \frac{\partial r_3}{\partial X_c} = \frac{1}{6} \epsilon_{ipq} \epsilon_{jlm} \frac{\partial r_i}{\partial X_j} \frac{\partial r_p}{\partial X_l} \frac{\partial r_q}{\partial X_m} \quad (\text{A3})$$

and ϵ_{ijk} is the usual Levi-Civita symbol. Define $\hat{L}[\mathbf{A}, \mathbf{B}, \mathbf{C}] = \epsilon_{lmq} \epsilon_{ijk} \frac{\partial A_i}{\partial X_l} \frac{\partial B_j}{\partial X_m} \frac{\partial C_k}{\partial X_q}$. This gives

$$\nabla_{\mathbf{r}} \cdot \ddot{\mathbf{r}} = \frac{1}{2J} \epsilon_{lmn} \epsilon_{ijk} \frac{\partial \ddot{r}_i}{\partial X_l} \frac{\partial r_j}{\partial X_m} \frac{\partial r_k}{\partial X_n} = \frac{1}{2J} \hat{L}[\ddot{\mathbf{r}}, \mathbf{r}, \mathbf{r}]. \quad (\text{A4})$$

The divergence equation then becomes

$$\frac{1}{2J} \hat{L}[\ddot{\mathbf{r}}, \mathbf{r}, \mathbf{r}] = -4\pi G \left(\frac{\rho_{m,0} a_0^3 (1 + \delta(\mathbf{X}, t_0))}{J} + \rho_{X,0} (1 + 3w) \left(\frac{a_0}{a} \right)^{3(1+w)} \right). \quad (\text{A5})$$

Using the standard definitions of $\Omega_{m,0}$, $\Omega_{X,0}$, H_0 , multiplying by J and noting that $J = \frac{1}{6} \hat{L}[\mathbf{r}, \mathbf{r}, \mathbf{r}]$, the equation is

$$\hat{L}[\ddot{\mathbf{r}}, \mathbf{r}, \mathbf{r}] = -3H_0^2 \Omega_{m,0} a_0^3 (1 + \delta(\mathbf{X}, t_0)) - \frac{H_0^2}{2} (1 + 3w) \Omega_{X,0} \left(\frac{a_0}{a} \right)^{3(1+w)} \hat{L}[\mathbf{r}, \mathbf{r}, \mathbf{r}]. \quad (\text{A6})$$

The gravitational field is irrotational in Eulerian space so $(\nabla_r \times \ddot{\mathbf{r}}) = \mathbf{0}$. Consider the component of equation (13) along the i -th direction. Again use (A2) to write

$$(\nabla_r \times \ddot{\mathbf{r}})_i = \epsilon_{ijk} \frac{\partial \ddot{r}_k}{\partial r_j} = \epsilon_{ijk} \frac{\partial \ddot{r}_k}{\partial X_l} \frac{\partial X_l}{\partial r_j} = \frac{1}{2J} \epsilon_{ijk} \epsilon_{lmn} \epsilon_{jrs} \frac{\partial \ddot{r}_k}{\partial X_l} \frac{\partial r_r}{\partial X_m} \frac{\partial r_s}{\partial X_n} = 0. \quad (\text{A7})$$

Using the identity $\epsilon_{ijk} = -\epsilon_{jik}$ and $\epsilon_{jik} \epsilon_{jrs} = \delta_{ir} \delta_{ks} - \delta_{is} \delta_{kr}$ in the above equation

$$-\epsilon_{lmn} \frac{\partial \ddot{r}_k}{\partial X_l} \frac{\partial r_i}{\partial X_m} \frac{\partial r_k}{\partial X_n} + \epsilon_{lmn} \frac{\partial \ddot{r}_k}{\partial X_l} \frac{\partial r_k}{\partial X_m} \frac{\partial r_i}{\partial X_n} = 2\epsilon_{lmn} \frac{\partial \ddot{r}_k}{\partial X_l} \frac{\partial r_k}{\partial X_m} \frac{\partial r_i}{\partial X_n} = 0. \quad (\text{A8})$$

Here we have set each component of the vector $\nabla_r \times \ddot{\mathbf{r}}$ in the r basis equal to zero. One can also express the components of $\nabla_r \times \ddot{\mathbf{r}}$ in the X basis where the two bases are related by $\hat{r}_i = \frac{\partial X_p}{\partial r_i} \hat{X}_p$. This gives

$$\epsilon_{lmn} \frac{\partial \ddot{r}_k}{\partial X_l} \frac{\partial r_k}{\partial X_m} \frac{\partial r_i}{\partial X_n} \frac{\partial X_p}{\partial r_i} \hat{X}_p = 0. \quad (\text{A9})$$

But $\partial r_i / \partial X_n \cdot \partial X_p / \partial r_i = \delta_{pn}$. Since the basis vectors are all independent the individual components must be zero. The simplified condition for each n then becomes

$$\epsilon_{nlm} \frac{\partial \ddot{r}_k}{\partial X_l} \frac{\partial r_k}{\partial X_m} = 0. \quad (\text{A10})$$

Defining $\hat{T}_q[\mathbf{A}, \mathbf{B}] = \epsilon_{lmq} \frac{\partial A_k}{\partial X_l} \frac{\partial B_k}{\partial X_m}$ it is rewritten as $\hat{\mathbf{T}}[\ddot{\mathbf{r}}, \mathbf{r}] = \mathbf{0}$. \hat{L} and $\hat{\mathbf{T}}$ are linear in each of their variables.

APPENDIX B: COMPUTATIONAL DETAILS OF THE EB SCHEME

In the EB frame, the equations to be solved have the following form

$$D_t^L [\nabla_{\mathbf{X}} \cdot \mathbf{p}^{(1)}] = -\frac{3}{2} H_0^2 \Omega_{m,0} a_0^3 \delta(\mathbf{X}, t_0) \quad (\text{B1})$$

$$D_t^T [\nabla_{\mathbf{X}} \times \mathbf{p}^{(1)}] = 0 \quad (\text{B2})$$

$$D_t^L [\nabla_{\mathbf{X}} \cdot \mathbf{p}^{(n)}] = S^{(n,L)} \quad (\text{B3})$$

$$D_t^T [\nabla_{\mathbf{X}} \times \mathbf{p}^{(n)}] = \mathbf{S}^{(n,T)}, \quad (\text{B4})$$

where n refers to orders higher than the first and

$$D_t^L = \left(2a\ddot{a} + \frac{3}{2}a^2H_0^2(1+3w)\Omega_{X,0} \left(\frac{a_0}{a}\right)^{3(1+w)} + a^2\frac{d^2}{dt^2} \right) \quad (\text{B5})$$

$$D_t^T = \left(-\ddot{a} + a\frac{d^2}{dt^2} \right). \quad (\text{B6})$$

The explicit form for the source terms is

$$\begin{aligned} S^{(n,L)} &= \sum_{\substack{\alpha,\beta \\ \alpha+\beta=n}} \left(-\frac{1}{2}\ddot{a} - \frac{3}{4}aH_0^2(1+3w)\Omega_{X,0} \left(\frac{a_0}{a}\right)^{3(1+w)} \right) \hat{L}[\mathbf{p}^{(\alpha)}, \mathbf{p}^{(\beta)}, \mathbf{X}] \\ &\quad - \sum_{\substack{\alpha,\beta \\ \alpha+\beta=n}} a\hat{L}[\ddot{\mathbf{p}}^{(\alpha)}, \mathbf{p}^{(\beta)}, \mathbf{X}] - \sum_{\substack{\alpha,\beta,\gamma \\ \alpha+\beta+\gamma=n}} \frac{1}{2}\hat{L}[\ddot{\mathbf{p}}^{(\alpha)}, \mathbf{p}^{(\beta)}, \mathbf{p}^{(\gamma)}] \\ &\quad - \sum_{\substack{\alpha,\beta,\gamma \\ \alpha+\beta+\gamma=n}} \frac{1}{4}H_0^2(1+3w)\Omega_{X,0} \left(\frac{a_0}{a}\right)^{3(1+w)} \hat{L}[\mathbf{p}^{(\alpha)}, \mathbf{p}^{(\beta)}, \mathbf{p}^{(\gamma)}] \end{aligned} \quad (\text{B7})$$

$$\mathbf{S}^{(n,T)} = - \sum_{\substack{\alpha,\beta \\ \alpha+\beta=n}} \hat{\mathbf{T}}[\ddot{\mathbf{p}}^{(\alpha)}, \mathbf{p}^{(\beta)}], \quad (\text{B8})$$

where α, β, γ can take any values from 1 to $n-1$ and they add up to n . These are subject to initial conditions

$$\text{at first order } \mathbf{p}^{(1,L/T)}(\mathbf{X}, t_0) = 0, \quad \dot{\mathbf{p}}^{(1,L/T)}(\mathbf{X}, t_0) = \mathbf{v}^{L/T}(\mathbf{X}, t_0) \quad (\text{B9})$$

$$\text{at higher order } \mathbf{p}^{(n,L/T)}(\mathbf{X}, t_0) = 0, \quad \dot{\mathbf{p}}^{(n,L/T)}(\mathbf{X}, t_0) = 0. \quad (\text{B10})$$

Since the spatial and temporal operators in equations (B1) - (B4) commute, the displacement field can be written as a linear combination spatial vectors with purely time dependent coefficients

$$\mathbf{p}^{(n,L/T)} = \sum_{i=1}^{Z_{n,L/T}} b_i^{(n,L/T)} \mathbf{F}_i^{(n,L/T)}, \quad (\text{B11})$$

where b and \mathbf{F} are functions of t and \mathbf{X} respectively i.e., $b \equiv b(t)$ and $\mathbf{F} \equiv \mathbf{F}(\mathbf{X})$ and $Z_{n,L}$ ($Z_{n,T}$) denote the number of independent longitudinal (transverse) terms at the n -th order. The superscripts denote the order and type of the term. Using this decomposition, one can denote the higher order source terms as

$$S^{(n,L)} = \sum_{i=1}^{Z_{n,L}} h_i^{(n,L)}(t) \cdot \hat{L}_i[\mathbf{F}^\alpha, \mathbf{F}^\beta, \mathbf{F}^\gamma] \quad (\text{B12})$$

$$\mathbf{S}^{(n,T)} = \sum_{i=1}^{Z_{n,T}} h_i^{(n,T)}(t) \cdot \hat{\mathbf{T}}_i[\mathbf{F}^\alpha, \mathbf{F}^\beta] \quad (\text{B13})$$

respectively, where the superscripts of \mathbf{F} s take any value between 0 to $n-1$ (0 corresponding to $\mathbf{F}(\mathbf{X}) = \mathbf{X}$) and add up to n . It is possible to calculate all the independent spatial source terms symbolically at all orders using the symmetries and properties of the \hat{L} and $\hat{\mathbf{T}}$ from which the numbers $Z_{n,L}$ and $Z_{n,T}$ can be determined and temporal source functions $h(t)$ can be extracted.

The initial perturbation is described by one scalar field $\delta(\mathbf{X}, t_0)$ corresponding to the initial density field in the EB frame and two vector fields $\mathbf{v}^L(\mathbf{X}, t_0)$ and $\mathbf{v}^T(\mathbf{X}, t_0)$ corresponding respectively to the curl-free and divergence-less parts of the initial velocity field (in the EB frame). The initial acceleration vector can be constructed from the initial density field via Poisson's equation and is also curl-free. This gives $Z_{1,L} = 2$ and $Z_{1,T} = 1$. Table B1 shows the number of terms at various orders. If the initial conditions start with zero transverse velocity then $Z_{1,T} = 0$. In this special case the total number of equations to solve reduces from 9 to 4 at second order and from 64 to 20 at third order.

Substituting equation (B11) up to first order in equations (B1) and (B2) gives,

$$D_t^L b_1^{(1,L)}[\nabla_{\mathbf{X}} \cdot \mathbf{F}_1^{(1,L)}] + D_t^L b_2^{(1,L)}[\nabla_{\mathbf{X}} \cdot \mathbf{F}_2^{(1,L)}] = -\frac{3}{2}H_0^2\Omega_{m,0}a_0^3\delta(\mathbf{X}, t_0), \quad (\text{B14})$$

Table B1. Number of transverse and longitudinal terms as a function of Lagrangian order and type of initial conditions.

Order	Zel'dovich initial conditions	$\mathbf{v}^T = 0$	$\mathbf{v}^T \neq 0$
n=1	$Z_L = 2, Z_T = 0$	$Z_L = 2, Z_T = 0$	$Z_L = 2, Z_T = 1$
n=2	$Z_L = 3, Z_T = 0$	$Z_L = 3, Z_T = 1$	$Z_L = 6, Z_T = 3$
n=3	$Z_L = 10, Z_T = 6$	$Z_L = 12, Z_T = 8$	$Z_L = 37, Z_T = 27$

$$D_t^T b_1^{(1,T)} [\nabla_X \times \mathbf{F}_1^{(1,T)}] = 0. \quad (\text{B15})$$

The initial conditions that $\mathbf{p}^{(1)}$ satisfies are given by equations (B9). There is a choice to be made in how these initial conditions translate to conditions on the temporal and spatial functions. We choose to set them as shown below.

$$\begin{aligned} \nabla_X \cdot \mathbf{F}_1^{(1,L)} &= \delta(\mathbf{X}, t_0) & \mathbf{F}_2^{(1,L)} &= \mathbf{v}^L(\mathbf{X}, t_0) & \mathbf{F}_1^{(1,T)} &= \mathbf{v}^T(\mathbf{X}, t_0) \\ D_t^L b_1^{(1,L)} &= -\frac{3}{2} H_0^2 \Omega_{m,0} a_0^3 & D_t^L b_2^{(1,L)} &= 0 & D_t^T b_1^{(1,T)} &= 0. \\ b_1^{(1,L)}(t_0) &= 0 & b_2^{(1,L)}(t_0) &= 0 & b_1^{(1,T)}(t_0) &= 0 \\ \dot{b}_1^{(1,L)}(t_0) &= 0 & \dot{b}_2^{(1,L)}(t_0) &= 1 & \dot{b}_1^{(1,T)}(t_0) &= 1 \end{aligned}$$

Substituting equation (B11) in the higher order equations equations (B3) and (B4) and imposing equation (B10) gives

$$\begin{aligned} \nabla_X \cdot \mathbf{F}_i^{(n,L)} &= \hat{L}_i[\mathbf{F}^\alpha, \mathbf{F}^\beta, \mathbf{F}^\gamma] & \nabla_X \times \mathbf{F}_i^{(n,T)} &= \hat{\mathbf{T}}_i[\mathbf{F}^\alpha, \mathbf{F}^\beta]. \\ D_t^L b_i^{(n,L)}(t) &= h_i^{(n,L)}(t) & D_t^T b_i^{(n,T)}(t) &= h_i^{(n,T)}(t). \\ b_i^{(n,L)}(t_0) &= 0 & b_i^{(n,T)}(t_0) &= 0. \\ \dot{b}_i^{(n,L)}(t_0) &= 0 & \dot{b}_i^{(n,T)}(t_0) &= 0. \end{aligned}$$

All the spatial solutions are subject to periodic boundary conditions and are solved using Fourier transforms.

APPENDIX C: FORMAL REQUIREMENTS OF THE EB SOLUTION

The formal derivation by Ehlers and Buchert (EB97) demands that the displacement in the EB frame satisfies

$$\int_V \mathbf{p}(\mathbf{X}, t) d^3 X = 0. \quad (\text{C1})$$

for all times t . At the initial time the definition of the Lagrangian coordinate implies $\mathbf{p}(\mathbf{X}, t_0) = 0$ and equation (C1) is trivially satisfied. We want to prove that if the initial data satisfies

$$\langle \delta(\mathbf{X}, t_0) \rangle_X = 0 \quad (\text{C2})$$

$$\langle \mathbf{v}(\mathbf{X}, t_0) \rangle_X = 0 \quad (\text{C3})$$

and the system is periodic, then equation (C1) holds at all times. We refer to these as the ‘zero-mean’ initial conditions.

Proof: The displacement $\mathbf{p}(\mathbf{X}, t)$ is a time-dependent linear combination of some spatial functions $\mathbf{F}(\mathbf{X})$. We will prove that each $\mathbf{F}(\mathbf{X})$ satisfies $\langle \mathbf{F}(\mathbf{X}) \rangle_X = 0$ and therefore $\langle \mathbf{p}(\mathbf{X}, t) \rangle_X = 0$.

At first order, the spatial function is either a solution of $\nabla_X \cdot \mathbf{F}(\mathbf{X}) = \delta(\mathbf{X}, t_0)$ or $\mathbf{F}(\mathbf{X}) = \mathbf{v}(\mathbf{X}, t_0)$. Since the initial density integrates to zero over the volume and the system is periodic, the solution also has the same property. Therefore, at first order all spatial \mathbf{F} s has mean zero.

At higher orders the \mathbf{F} s are periodic solutions of $\nabla_X \cdot \mathbf{F} = S^L(\mathbf{X})$ or $\nabla_X \times \mathbf{F} = \mathbf{S}^T(\mathbf{X})$, where S^L, \mathbf{S}^T are combinations of lower order \mathbf{F} s. So if $S^L(\mathbf{X})$ and $\mathbf{S}^T(\mathbf{X})$ have zero mean then periodicity will imply that each higher order \mathbf{F} has mean zero. Here we present the proof only for the longitudinal source terms $S^L(\mathbf{X}) = \hat{L}[\mathbf{F}^\alpha, \mathbf{F}^\beta, \mathbf{F}^\gamma]$. The proof for the transverse sources $\hat{\mathbf{T}}[\mathbf{F}^\alpha, \mathbf{F}^\beta]$ follows a similar calculation.

Let $I = \langle \hat{L}[\mathbf{F}^\alpha, \mathbf{F}^\beta, \mathbf{F}^\gamma] \rangle$. To keep in mind the periodic nature of the system, we refer to space as the 3-torus \mathbf{T}^3 . Write $I = \frac{1}{V} \epsilon_{ijk} I'_{ijk}$, where

$$I'_{ijk} = \epsilon_{pqr} \int_{\mathbf{T}^3} d^3 X \frac{\partial F_i^\alpha}{\partial X_p} \frac{\partial F_j^\beta}{\partial X_q} \frac{\partial F_k^\gamma}{\partial X_r}. \quad (\text{C4})$$

Here the spatial functions \mathbf{F} can either be periodic functions of \mathbf{X} or equal to \mathbf{X} . These are higher order source terms. Hence at least one of \mathbf{F} s is not \mathbf{X} . Without loss of generality let this correspond to the term $\partial F_k / \partial X_r$. Integrating by parts over X_r and using periodicity gives

$$I'_{ijk} = -\epsilon_{pqr} \int_{\mathbf{T}^3} d^3X \frac{\partial}{\partial X_r} \left(\frac{\partial F_i^\alpha}{\partial X_p} \frac{\partial F_j^\beta}{\partial X_q} \right) F_k^\gamma = -\epsilon_{pqr} \int_{\mathbf{T}^3} d^3X \left[\left(\frac{\partial^2 F_i^\alpha}{\partial X_r \partial X_p} \right) \frac{\partial F_j^\beta}{\partial X_q} + \left(\frac{\partial^2 F_j^\beta}{\partial X_r \partial X_q} \right) \frac{\partial F_i^\alpha}{\partial X_p} \right] F_k^\gamma. \quad (\text{C5})$$

The first integrand is symmetric under the exchange $r \leftrightarrow p$ and the second under the exchange $r \leftrightarrow q$. ϵ_{pqr} is antisymmetric under these exchanges. Therefore, $I'_{ijk} = 0$ and hence $I = 0$. Similarly one can show that the source terms for solving the transverse vectors also integrate to zero. Thus equation (C1) holds for all t .

APPENDIX D: SETTING THE INITIAL CONDITIONS ALONG THE ZEL'DOVICH CURVE

It is generally common in cosmology to assume that the initial velocity is proportional to the initial acceleration (Zel'dovich 1970); the proportionality constant is set by requiring that there be no perturbations at the big bang. This is also equivalent to having no decaying modes i.e. no negative powers of t in the displacement. At very early times (recombination) the universe is purely matter dominated with $\Omega = 1$ and the first order displacement evolves as (B92)

$$\mathbf{p}^{(1)} = \left(\frac{t}{t_0} \right)^{-1/3} \left[-\frac{2a_0}{5} \mathbf{F}_1^{(1,L)} - \frac{3t_0}{5} \mathbf{v}^L \right] + \left(\frac{t}{t_0} \right)^{4/3} \left[-\frac{3a_0}{5} \mathbf{F}_1^{(1,L)} + \frac{3t_0}{5} \mathbf{v}^L \right] + a_0 \left(\frac{t}{t_0} \right)^{2/3} \mathbf{F}_1^{(1,L)}. \quad (\text{D1})$$

Setting the coefficient of the negative power of t to zero gives

$$\mathbf{v}^L = -\frac{2}{3} \cdot \frac{a_0}{t_0} \mathbf{F}_1^{(1,L)} = -\dot{a}(t_0) \mathbf{F}_1^{(1,L)}. \quad (\text{D2})$$

Note that this does not guarantee that there are no decaying modes from the higher order solution. The terms $(t/t_0)^{-1/3}$ and $(t/t_0)^{4/3}$ arise from the homogeneous part of the solution and each higher order solution will contain them since the temporal derivative operator is the same at all orders. An alternate way is to choose the initial velocity such that the scaled velocity divergence $\delta v = (3H_0)^{-1} \nabla_{r_{OBS}} \cdot \mathbf{v}_{OBS}$ and $\delta(\mathbf{X}, t_0)$ at each point satisfy the non-linear Zel'dovich relation based on the top-hat analysis (NC11). In this case the relationship in equation (D2) is not satisfied; decaying modes will be present even at first order. The former prescription is used more often in literature and in this paper. We also checked that the difference in the two ways of setting the initial conditions is very small ($\sim 10^{-8}$) when the starting epoch is $z \sim 1000$ (recombination).

APPENDIX E: 1D PERTURBATIONS

This appendix proves the results for the 1-D case stated in §3.3.

E1 Frame shift for a single step

Since the problem is essentially 1-d, we will denote all spatial functions as scalar functions. The Lagrangian coordinate in the observer (EB) frame is denoted as Y (X); $Y = X$. The initial density and velocity in the observer frame are $\delta_{OBS}(Y, t_0)$ and $v_{OBS}(Y, t_0)$ respectively. The initial data in the EB frame is

$$\delta_{EB}(X, t_0) = \delta_{OBS}(Y, t_0); \quad v_{EB}(X, t_0) = v_{OBS}(Y, t_0) - v_{c,0}, \quad (\text{E1})$$

where $v_{c,0} = \langle v_{OBS}(Y, t_0) \rangle$. The acceleration in the observer's frame is given by $F_\delta(Y, t_0)$ where $dF_\delta/dY = \delta_{OBS}(Y, t_0)$. The densities are the same, hence $F_\delta(X, t_0) = F_\delta(Y, t_0)$. Hereafter we drop the subscripts on the density since it is the same in both frames.

The displacement in the EB frame at any later time is given as

$$p(X, t) = b_1(t)F_1(X) + b_2(t)F_2(X), \quad (\text{E2})$$

where $F_1(X) = F_\delta(X, t_0)$ and $F_2(X) = v_{EB}(X, t_0)$. The physical coordinate

$$r_{EB}(X, t) = aX + p(X, t) \quad (\text{E3})$$

and the corresponding Jacobian is

$$J(X, t) = a^3 \left(1 + \frac{1}{a} \frac{dp}{dX} \right). \quad (\text{E4})$$

The comoving coordinate is $x_{EB} = r_{EB}/a$. Restricting to 1D and substituting equation (E3) and (E4) in equation (56), the frameshift equation is

$$\frac{d}{dt} \left(a^2 \frac{d\Delta x}{dt} \right) = -\frac{1}{L} \int (a\ddot{p} - \ddot{a}p) \left(1 + \frac{1}{a} \frac{dp}{dX} \right) dX. \quad (\text{E5})$$

Since p is a periodic function of X , this gives

$$\frac{d}{dt} \left(a^2 \frac{d\Delta x}{dt} \right) = -\frac{1}{L} \int \dot{p} \frac{dp}{dX} dX. \quad (\text{E6})$$

Substituting for p from equation (E2)

$$\frac{d}{dt} \left(a^2 \frac{d\Delta x}{dt} \right) = -\frac{1}{L} \int (\ddot{b}_1 b_2 F_1 F_2' + \ddot{b}_2 b_1 F_2 F_1') dX, \quad (\text{E7})$$

where prime denotes differentiation w.r.t. X or Y . Using the equations for \ddot{b}_1 and \ddot{b}_2 given in Appendix B, applying the product rule for derivatives and using periodicity of the spatial functions gives

$$\frac{d}{dt} \left(a^2 \frac{d\Delta x}{dt} \right) = - \left(3\ddot{a} + \frac{3}{2}(1+3w)a\Omega_{X,i} \left(\frac{a_i}{a} \right)^{3(1+w)} \right) b_2 \frac{1}{L} \int (F_1 F_2') dX \propto \int F_\delta(Y, t_0) v'_{OBS}(Y, t_0) dY, \quad (\text{E8})$$

with initial conditions $\Delta x(t_0) = 0$ and $\dot{\Delta x}(t_0) = v_{c,0}/a_0$. Consider the case where $v_{OBS}(Y, t_0) \propto F_\delta(Y, t_0)$. The condition that the mean density be zero implies $\langle F_\delta(Y, t_0) \rangle = v_{c,0} = 0$. Thus the initial conditions as well as source term of equation (E8) are zero and hence $\Delta x = 0$ for all t . Thus, single step LPT with Zel'dovich initial conditions requires no shifts.

E2 Maintaining the Zel'dovich condition

Let the initial time at the start at the first step be t_0 and consider taking a second step at time t_1 . Let Y_0, Y_1 be the Lagrangian coordinates in the observer frame at time t_0, t_1 respectively. Y_1 is related to Y_0 as

$$Y_1 = Y_0 + a^{-1} p(X, t_1) + \Delta x(t_1) \quad (\text{E9})$$

If $v_{OBS}(Y_0, t_0) \propto F_\delta(Y_0, t_0)$, then $v_{c,0} = 0$ and $v_{EB}(X, t_0) = v_{OBS}(Y_0, t_0)$. Combining with equation (E2), this gives

$$p(X, t_1) \propto F_\delta(Y_0, t_0) \quad \text{and} \quad \dot{p}(X, t_1) \propto F_\delta(Y_0, t_0). \quad (\text{E10})$$

The velocity in the observer frame at the start of the second step is

$$v_{OBS}(Y_1, t_1) = \dot{p}(X, t_1) - \frac{\dot{a}(t_1)}{a(t_1)} p(X, t_1) + a \dot{\Delta x}(t_1). \quad (\text{E11})$$

The acceleration at the start of the second step is

$$F_\delta(Y_1, t_1) = \int \delta(Y_1, t_1) dY_1 = \frac{(1 + \delta(Y_0, t_0)) a^3}{J(X, t)} - 1, \quad (\text{E12})$$

where $J(X, t)$ is given by equation (E4). Transforming from Y_1 to $X(= Y_0)$ using equation (E9)

$$F_\delta(Y_1, t_1) = \int (1 + \delta(Y_0, t_0)) dY_0 - \int \left(1 + \frac{1}{a} \frac{dp}{dX} \right) dX \quad (\text{E13})$$

$$= F_\delta(Y_0, t_0) - \frac{p(X, t_1)}{a}. \quad (\text{E14})$$

When the initial acceleration and velocity are proportional, the above equation can be combined with equation (E10) to give $F_\delta(Y_1, t_1) \propto F_\delta(Y_0, t_0)$. Since the frame shifts are zero, equation (E10) and (E11) give $v_{OBS}(Y_1, t_1) \propto F_\delta(Y_0, t_0)$. This proves that if the initial acceleration and velocity are proportional they remain proportional at all subsequent times.

E3 Conservation of mean velocity

Using the periodicity of $p(X, t)$, equation (E6) can be re-written as

$$\frac{d}{dt} \left(a^2 \frac{d\Delta x}{dt} \right) = \frac{d}{dt} \left(-\frac{1}{L} \int \dot{p} \frac{dp}{dX} dX \right). \quad (\text{E15})$$

This gives

$$\dot{\Delta x}(t) = \frac{v_{c,0} a_0}{a^2} - \frac{1}{a^2} \left(\frac{1}{L} \int \dot{p} \frac{dp}{dX} dX \right). \quad (\text{E16})$$

The velocity in the observer frame at any time is given by equation (E11). The mean at any time t is

$$\langle v_{OBS}(Y_1, t) \rangle = \frac{1}{L} \int v_{OBS}(Y_1, t) dY_1 \quad (\text{E17})$$

$$= \frac{1}{L} \int \left(\dot{p} - \frac{\dot{a}}{a} p + a \dot{\Delta x} \right) \left(1 + \frac{1}{a} \frac{dp}{dX} \right) dX \quad (\text{E18})$$

$$= a \dot{\Delta x} + \frac{1}{a} \left(\frac{1}{L} \int \dot{p} \frac{dp}{dX} dX \right). \quad (\text{E19})$$

Substituting for $\dot{\Delta}x$ from equation (E16),

$$\langle v_{OBS}(Y_1, t) \rangle = \frac{v_{c,0} a_0}{a}. \quad (\text{E20})$$

Thus, for a 1-d system the mean velocity, like the mean momentum, is conserved modulo a ‘1/a decay’ due to the Hubble drag.

APPENDIX F: SPHERICAL TOP-HAT

This section describes the details involved in setting up the compensated top-hat configuration for section 3.5.

The exact compensated top-hat function consists of a spherical overdense region surrounded by a compensating underdense vacuum region. Let a and b be the radii of the overdense and compensating regions respectively. The initial density profile is given by

$$\delta(\mathbf{X}, t_0) = \begin{cases} \delta_0 & 0 \leq |\mathbf{X}| < a \\ -1 & a \leq |\mathbf{X}| < b \\ 0 & |\mathbf{X}| \geq b \end{cases} \quad (\text{F1})$$

We chose $\delta_0 = 10$, $a = 1/4$ and $b = 11^{1/3}/4$. The box length L_{box} is chosen to be two units in length centred around the point $(1/10, -1/11, 1/(2\pi))$. The choice of parameters ensures that the entire profile is well represented within the box and the offset ensures that no special symmetry is exploited in the test. The profile is discontinuous at $X = a$ and $X = b$. The Fourier transform of a discontinuous function has power at all wave numbers and the Gibbs phenomenon prevents such functions from being completely represented by Fourier transforms on any finite size grid. The initial profile is hence smoothed with a Gaussian filter of width σ to give

$$\delta_\sigma(\mathbf{X}, t_0) = \int_0^{L_{box}} \delta(\mathbf{X}, t_0) \cdot \frac{\exp(-X^2/2\pi\sigma^2)}{(2\pi\sigma^2)^{3/2}} d^3X. \quad (\text{F2})$$

The smoothing is performed analytically in real space and the resulting function is numerically evaluated on the grid. To ensure periodicity of the initial data, contribution of the 26 nearest neighbours cells is added. The contribution of cells beyond the nearest neighbours was zero to machine precision. For the density profile in §3.5, the smoothing parameter is $\sigma = 1/12$.

APPENDIX G: GENERATION OF THE TRANSVERSE VELOCITY

The Eulerian vorticity in the observer frame is $\nabla_{r_{OBS}} \times \mathbf{v}_{OBS}$.

$$\nabla_{r_{OBS}} \times \mathbf{v}_{OBS} = \epsilon_{ijk} \frac{\partial v_{OBS,k}}{\partial r_{OBS,j}}. \quad (\text{G1})$$

LPT expresses \mathbf{v}_{OBS} as functions of the Lagrangian variable \mathbf{Y} and not \mathbf{r}_{OBS} . Using the relations in Appendix A and properties of the Levi-Civita tensor gives

$$(\nabla_{r_{OBS}} \times \mathbf{v}_{OBS})_i = \frac{1}{2J} \epsilon_{ijk} \epsilon_{j pq} \epsilon_{lmn} r_{p,m} r_{q,n} v_{k,l} \quad (\text{G2})$$

$$= \frac{1}{2J} (\delta_{kp} \delta_{iq} - \delta_{ip} \delta_{kq}) \epsilon_{lmn} r_{p,m} r_{q,n} v_{k,l} \quad (\text{G3})$$

$$= \frac{1}{2J} \epsilon_{lmn} (r_{k,m} r_{i,n} v_{k,l} - r_{i,m} r_{k,n} v_{k,l}) \quad (\text{G4})$$

where the ‘comma’ denotes differentiation with respect to the Lagrangian variable $\mathbf{Y} = \mathbf{X}$. Substituting for \mathbf{r}_{OBS} and \mathbf{v}_{OBS} from equations (60) and (62) gives rise to three types of terms in the expression: $\{\epsilon_{ilk} \dot{p}_{k,l}, \epsilon_{ilk} p_{k,l}\}$, $\{\epsilon_{ilm} p_{k,n} \dot{p}_{k,l}\}$ and $\{\epsilon_{lmn} p_{i,m} p_{k,n} \dot{p}_{k,l}\}$. The first kind corresponds to the vorticity in the Lagrangian frame while the remaining two have no obvious physical interpretation. In general, all three types of terms are non-zero. For a first order LPT calculation (i.e., the displacement is accurate to first order in the expansion parameter and leading errors are second order), $\dot{\mathbf{p}}$ is always proportional to \mathbf{p} and the anti-symmetry of the Levi-Civita tensor ensures that all three types of terms vanish. The second order LPT series does not have this feature. In particular, the second order displacement term in the series $\mathbf{p}^{(2)}$ is not proportional to the first order $\mathbf{p}^{(1)}$ and hence combinations of these (which are third order) will in general not be zero. Thus, the Eulerian vorticity will in general have non-zero contributions which are third order and higher (up to order 6) in the expansion parameter. Thus, when calculations are performed with second order LPT, the Eulerian vorticity is non-zero although the Lagrangian vorticity is zero.